Design of a High Temperature GaN-Based VCO for Downhole Communications

Tianming Feng

Thesis submitted to the faculty of the Virginia Polytechnic Institute and State University in partial fulfillment of the requirements for the degree of

Master of Science
In
Electrical and Engineering

Dong S. Ha
Kwang-Jin Koh
Dan M. Sable

December 15, 2016
Blacksburg, VA

Keywords: high temperature, extreme environment, VCO, GaN on SiC, downhole communications system

Design of a High Temperature GaN-Based VCO for Downhole Communications

Tianming Feng

Abstract

Decreasing reserves of natural resources drives the oil and gas industry to drill deeper and deeper to reach unexploited wells. Coupled with the demand for substantial real-time data transmission, the need for high speed electronics able to operating in harsher ambient environment is quickly on the rise. This paper presents a high temperature VCO for downhole communication system. The proposed VCO is designed and prototyped using 0.25 μm GaN on SiC RF transistor which has extremely high junction temperature capability. Measurements show that the proposed VCO can operate reliably under ambient temperature from 25 °C up to 230 °C and is tunable from 328 MHz to 353 Mhz. The measured output power is 18 dBm with ±1 dB variations over entire covered temperature and frequency range. Measured phase noise at 230 °C is from -121 dBc/Hz to -109 dBc/Hz at 100 KHz offset.

Design of a High Temperature GaN-Based VCO for Downhole Communications

Tianming Feng

General Audience Abstract

The oil and gas industry are drilling deeper and deeper to reach unexploited wells due to decreasing reserves of easily available natural resources. In addition, high speed electronics able to operating in harsher ambient environment is required to meet the demand for substantial real-time data transmission. This work presents a high temperature VCO for downhole communication system which can meet the requirement aforementioned. The proposed VCO is designed and prototyped to meet the harsh temperature and high speed requirement. Measurements show that, under ambient temperature from 25 °C up to 230 °C, the proposed VCO can operate reliably from 328 MHz to 353 Mhz, as required by the communication system.

Acknowledgements

I would like to thank Dr. Dong S. Ha for the opportunity to work on radio-frequency circuit project. I would also like to thank Dr. Kwang-Jin Koh and Dr. Dan M. Sable for serving on my defense committee and for the courses taught by them which help me to gain background in analog IC and op-amp circuit design.

I am grateful for the supporting work and resources provided by the Multifunctional Integrated Circuits and Systems (MICS) group and my colleagues. Without them, completion of this work would have been impossible.

Finally, I owe my achievements here to my parents. Virtues and everlasting love of them always inspire me and give me strength to overcome any difficulty.

Table of Contents

Table of Figures

Table of Tables

Chapter 1

1 Introduction

1.1 Application Background

Nowadays, the oil and gas industry need to drill deeper and deeper to reach previously unexploited wells. At the same time, the downhole environments are becoming harsher and reaching higher temperatures and pressures which necessitate more robust and higher speed electronics to reliably operate in these environments.

The main problem for downhole electronics is the temperature limitation, being that the pressures are handled mechanically. Despite wells being classified beyond 210 °C the current drilling temperatures do not exceed 200 °C [1]- [2]. This is due to that face that the current electronics, which made from Silicon, used in these systems can only operate upto 150 °C before being recovered from the well due to high leakage current. By increasing the ambient temperature capability of the electronic device, longer logging times and deeper drilling is capable. Cooling and conventional heat extraction techniques are impractical to use in downhole due to weight contribution, power consumption and added complexity.

In addition, the current telemetry systems use low frequency circuits that can achieve data rates of only approximately 4Mb/s at temperatures < 200 °C [1], which still does not meet the demand for rapid grown data rate due to higher resolution sensors, faster data logging speeds, and additional tool available for a downhole system. A radio frequency cable modem provides higher speed compare with the current systems [3]

An essential component in a RF cable modem is the VCO that generates RF carriers. There has been several oscillator designs [4] [5] [6] [7] and very few VCO designs operating at high temperature reported in the open literature.

This paper presents the first high temperature GaN HEMT VCO operating in UHF band at ambient temperature from 25 to 230 °C.

1.2 High Temperature Semiconductor Technology

Although relatively new in the commercial world, GaN was found to be the most promising technology for this application. GaN offers reliable combination of high temperature and high frequency capability. It also has been shown to be thermally robust and can have very low NF while simultaneously achieving high gain and high linearity. Although GaN is still in its nascent stages, the research into fabrication and reliability shows that it is a very promising technology. SiC, alone, can reach high temperature, but choosing a technology that operates at higher frequencies allows for the push into the radio and microwave bands, leading to much higher data rates.

To reduce power, the use of a transistor with small gate leakage current and low drain voltage allows for the low power control of the device current, which will be the primary factor in determining performance.

1.3 Summary

The VCO discussed herein has been designed as part of a downhole communication system under no existing limitations in frequency band or performance other than those determined through a system simulation.

The proposed VCO is designed and prototyped using 0.25 µm GaN on SiC RF transistor technology, which is chosen due to the high junction temperature capability. A common source colpitts oscillator was selected for topology. Measurements show that the proposed VCO can operate reliably up to an ambient temperature of 230 °C over frequency range 328 MHz to 350.5 MHz, output power of 17 dBm +- 0.5 dB and noise figure at -140 dBc/Hz at 1 MHz offset.

Chapter 2

2 Fundamentals of LC oscillator

Generally, oscillator can be designed in several ways for different applications and frequencies. Most commonly used are RC oscillator with op-amp, LC oscillator using a transistor amplifier and a LC tank as the resonator, and negative resistor oscillator which is commonly used in microwave frequency range. RC oscillator is often used in audio frequency range in applications like audio signal generator and electronic musical instrument. In frequency below 100 KHz, RC oscillator is more easily to be integrated in IC circuit since no bulky inductor is needed. LC oscillator, also called tuned-circuit oscillators are used commonly at frequencies larger than 100 KHz. The implementation of a high-Q resonator will make the oscillator generate less distortion and phase noise [8]. RC oscillator and LC oscillator can both be analyzed in feedback approach. However, in microwave frequency range or above, the parasitic of transistor plays an important role in determine the performance of transistor and the external LC can no longer determine the resonant frequency by themselves. Negative resistance oscillator design can overcome this issue. With the power of s-parameters and measuring techniques using Network Analyzer, oscillator design using negative resistance approach can be practically done [8]. This chapter will be primarily be about oscillator with LC tank feedback since this type of oscillator topology is employed in our design.

2.1 Time Domain Analysis of Oscillators

There are several commonly used approaches to analyze a potentially oscillating circuit, like time domain analysis, or by using feedback theory, or even using S-Parameters and related theory. However, time domain analysis provide us a unique perspective of how oscillation can start and achieve a stable oscillation state based on simple KCL law and nonlinear integral-differential

equations [9]. Typically, the nonlinear property stems from the intrinsic nonlinear device required in oscillator design. The integral and differential part of the equation is from the inductor and capacitor which both commonly used in LC oscillator design. Even though some numerical methods have been developed, a much easier approach to these nonlinear integral-differential equations is by using linear approximation. Even though not accurate, the solutions given by linear approximation can give us a good sense of principal behind oscillation.

2.1.1 Time Domain Analysis of Transformer-Coupled Oscillator

To better investigate the time domain approach for oscillator circuit analysis, a transformer coupled oscillator will be used as an example.

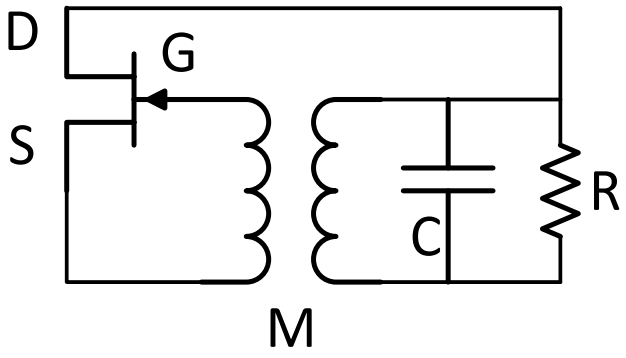

Figure 2.1 A transformer coupled oscillator [fair use]

The topology of transformer coupled oscillator is shown in the Figure 2.1 above. For simplicity, biasing circuit is ignored. We start with small signal analysis, zero initial state assumed. The MESFET is in common source connection. The small signal gate voltage is denoted by $v_g(t)$. $v_R(t)$ stands for the voltage cross resistor. Assuming ideal resistor, we can express the current flowing through R by

$$i_R(t) = \frac{v_R(t)}{R}$$

Similarly, assuming ideal capacitor C, we can get its current by

$$i_C(t) = C\frac{dv_R(t)}{dt}$$

The voltage across the resistor R and capacitor C is coupled to the gate terminal by the transformer, which is determined as

$$v_g(t) = \frac{M}{L} * v_R(t)$$

The MESFET works in saturation region. Again, the parasitic effects are ignored. So the impedance seen by the left brunch of transformer is infinite and then the current following through the transformer is negligible. The small signal trans-conductance of the MWSFET is denoted by $g_m(V)$.

By applying KCL law at the Drain terminal node, we can get equation

$$\frac{v_R(t)}{R} + C\frac{dv_R(t)}{dt} + \frac{1}{L}\int v_R(t)dt - i_D(t) = 0$$

Differentiating this equation we can get

$$\frac{1}{R}\frac{dv_R(t)}{dt} + C\frac{d^2v_R(t)}{dt^2} + \frac{1}{L}v_R(t) - \frac{di_D(t)}{dt} = 0$$

Since

$$\frac{di_D(t)}{dt} = \frac{di_D(t)}{dv_g(t)} * \frac{dv_g(t)}{dt}$$

and

$$v_R(t) = \frac{L}{M} * v_g(t)$$

substituting them into equation above, we can get

$$\frac{d^2v_g(t)}{dt^2} + \left(\frac{1}{RC} - \frac{g_m(v_g(t))M}{CL}\right) * \frac{dv_g(t)}{dt} + \frac{1}{LC} * v_g(t) = 0$$

The difficulty of solving the above equation is very dependent on the form of $g_m(v_g(t))$. In linear circuit operation, it is extensively considered as a constant for given biasing condition in small signal analysis. Under this assumption, we can find later by solving the second order differential equation that the solution is an everlastingly increasing sinusoid whose amplitude is also an exponential function with time. As mentioned forehead, oscillator is basically a nonlinear circuit. Actually, it is the nonlinearity of the trans-conductance of MESFET that makes the amplitude of the sinusoidal signal increase to certain value and then become stable. However, we still need to make the assumption of linear trans-conductance to get an analytical solution. And then from the linearity property, we can get a good idea of how the exponentially increasing signal can become stable.

Back to the second-order differential equation

$$\frac{d^2v_g(t)}{dt^2} + \left(\frac{1}{RC} - \frac{g_m(v_g(t))M}{CL}\right) * \frac{dv_g(t)}{dt} + \frac{1}{LC} * v_g(t) = 0$$

The characteristic equation is

$$r^2 + \left(\frac{1}{RC} - \frac{g_m(v_g(t))M}{CL}\right) * r + \frac{1}{LC} = 0$$

For simplicity, we use some of the denotations as below:

$$\omega_o = \frac{1}{\sqrt{LC}}$$

$$\delta = \left(\frac{1}{RC} - \frac{g_m(v_g(t))M}{CL}\right)$$

Then the characteristic equation can be simplified as

$$r^2 + \delta r + \omega_o^2 = 0$$

The solution of the characteristic equation is

$$r = \frac{-\delta \pm \sqrt{\delta^2 - 4\omega_o^2}}{2}$$

$$= -\frac{\delta}{2} \pm \sqrt{\left(\frac{\delta}{2}\right)^2 - \omega_o^2}$$

It's a good approximation that

$$-\omega_o < \delta \leq 0$$

Because when $\delta > 0$, the solution will be a decreasing sinusoid. While $\delta < -\omega_o$ is not possible, we don't need such a large gm to make an oscillator.

Based on that, we can rewrite expression of r as

$$r = -\frac{\delta}{2} \pm j\omega_o \sqrt{1 - \left(\frac{\delta}{\omega_o}\right)^2}$$

So the solution for the differential equation should be

$$v_g(t) = V_1 * e^{-\frac{\delta}{2}t} \cos\left(\sqrt{1 - \left(\frac{\delta}{\omega_o}\right)^2} * \omega_o t\right) + V_2 * e^{-\frac{\delta}{2}t} \sin\left(\sqrt{1 - \left(\frac{\delta}{\omega_o}\right)^2} * \omega_o t\right)$$

$$= V * e^{-\frac{\delta}{2}t} \cos(\omega_1 t - \varphi)$$

where V_1 and V_2 are constants, $V = \sqrt{V_1^2 + V_2^2}$, $\varphi = \arccos(\frac{V_1}{V})$, and $\omega_1 = \sqrt{1 - \left(\frac{\delta}{\omega_o}\right)^2} * \omega_o$.

The solution is a sinusoid with an exponentially increasing amplitude. In addition, both the frequency and speed of how fast the amplitude increasing are dependent on δ, or $g_m(v_g(t))$. The assumption of $\delta < 0$ simply implies that

$$\left(\frac{1}{RC} - \frac{g_m(v_g(t))M}{CL}\right) < 0$$

or

$$g_m\left(v_g(t)\right) > \frac{1}{R} * \frac{L}{M}$$

This is the so called start condition of LC oscillator. When oscillation starts and $v_g(t)$ increases, due to the nonlinearity of MESFET (or other transistor) device, the trans-conductance will decrease until it is equal to $\frac{1}{R} * \frac{L}{M}$. Then the amplitude of oscillation sinusoid becomes a constant. Also the oscillation frequency will reach ω_o since $\delta = 0$.

2.2.2 Time Domain Analysis of LC Colpitts Oscillator

Up to now, we have formed a sense of how time domain analysis can be used to examine the mechanism behind stable oscillation about how it starts and becomes stable. Also, it has been shown that how linear approximation of transistor trans-conductance can be used to solve the problematic second order differential equation and nonlinearity of it get a stable oscillation.

It's fortunate that the transformer coupled oscillator gives us a second order differential equation, which we only need to find the roots of quadratic equation to solve it based on linear approximation. However, for a pure LC oscillator, like colpitts oscillator, it often contain three inductors or capacitors totally, which means that we need to solve a nonlinear third order differential equation, or a cubic equation based on linear approximation. As we know, the roots of cubic equation are much more complicated than that of quadratic equation. The common source colpitts is used as example here to see how limited the time-domain analysis is.

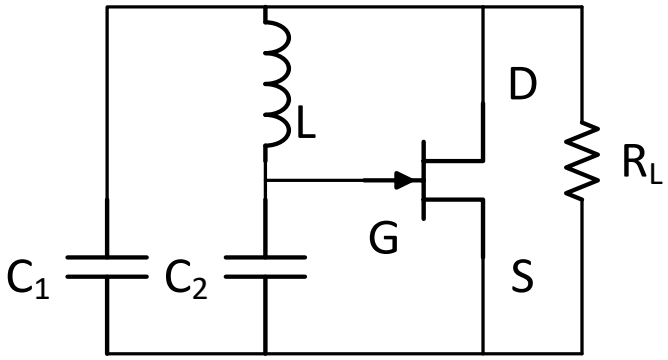

Figure 2.2 An LC Colpitts Oscillator [fair use]

The KCL equation can be written as

$$C_1 * \frac{dv_R(t)}{dt} + C_2 * \frac{dv_g(t)}{dt} + g_m V_g(t) + \frac{V_R(t)}{R_L} = 0$$

The current flowing into the gate is ignored.

The relationship between $v_R(t)$ and $v_g(t)$ can be found from

$$\begin{aligned} v_R(t) - v_g(t) &= L * \frac{di_L(t)}{dt} \\ &= L * \frac{di_{C_2}(t)}{dt} \\ &= L * \frac{d\left[C_2 * \frac{dv_g(t)}{dt}\right]}{dt} \\ &= L * C_2 * \frac{d^2 v_g(t)}{dt^2} \end{aligned}$$

Then $v_R(t)$ can be expressed by $v_g(t)$ as

$$v_R(t) = v_g(t) + L * C_2 * \frac{d^2 v_g(t)}{dt^2}$$

The KCL equation can be rewritten as

$$LC_1C_2\frac{d^3 v_g(t)}{dt^3} + \frac{LC_2}{R} * \frac{d^2 v_g(t)}{dt^2} + (C_1 + C_2) * \frac{dv_g(t)}{dt} + \left(g_m + \frac{1}{R}\right) * v_g(t) = 0$$

$$\frac{d^3 v_g(t)}{dt^3} + \frac{1}{RC_1} * \frac{d^2 v_g(t)}{dt^2} + \frac{C_1 + C_2}{LC_1C_2} * \frac{dv_g(t)}{dt} + \frac{1}{LC_1C_2}\left(g_m + \frac{1}{R}\right) v_g(t) = 0$$

The characteristic equation is

$$r^3 + \frac{1}{RC_1} * r^2 + \frac{1}{L} * \frac{C_1 + C_2}{C_1C_2} * r + \frac{1}{LC_1C_2}\left(g_m + \frac{1}{R}\right) = 0$$

It’s a cubic function the solution of which is so complicated that no clear perspective of the oscillation can be reasoned.

The numerical solution of time-domain nonlinear circuit can be found by using specific algorithm, which is out of the knowledge of the author.

Except for time-domain analysis, a less complicate approach is by using feedback theory. Even though much of detail behind the mechanism is ignored, we are still able to find the start-up condition and frequency of oscillation from this approach.

2.2 LC Tuned Oscillator Analyzed Using Feedback Theory.

LC tuned oscillators are broadly used in radio frequency range. It includes Armstrong Oscillator (also known as the Meissner oscillator), Clapp oscillator, Colpitts oscillator, Hartley oscillator and so on.

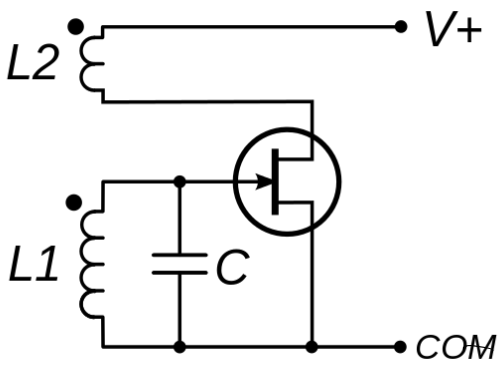

Figure 2.3 Topology of Armstrong oscillator using an FET [fair use]

Shown above is the Armstrong oscillator Figure 2.3 with triode vacuum tube in original design replaced by field-effect transistor in modern implementation. By exchanging the LC resonant with the feedback coil L2, we can get the Meissner oscillator, which is just the transformer coupled oscillator that we have discussed in the time-domain analysis.

Clapp oscillator, Colpitts and Hartley oscillator can be referred as Colpitts type oscillator, or sometime three-point oscillator. The similarity between Colpitts type oscillator is that it normally contains one transistor as active source and three reactant components, either two capacitors with one inductor, or two inductors with one capacitor. In addition to the variation of the combination of inductor and capacitor, there are three ways regarding how the transistor is connected, which are common-source, common-gate and common-drain. The transistor in original colpitts oscillator

is in common-drain connection with two capacitors and one inductor. In Clapp oscillator a variable capacitor (varactor) is added in series with the inductor to achieve variable frequency of oscillation without effecting the loop gain. In Hartley oscillator, the transistor is in common-source connection and in the LC tank feedback loop there are two inductors and one capacitor.

General Topology for Three Point Oscillator

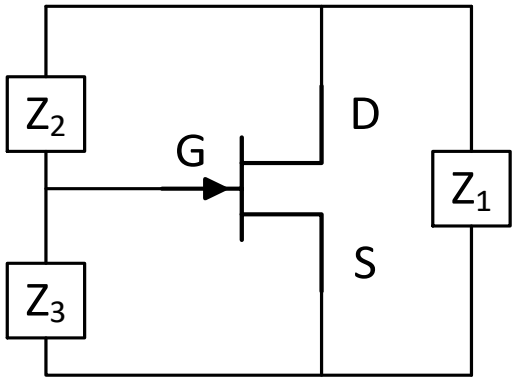

Figure 2.4 Topology of three-point oscillator

Figure 2.4 above is the general three-point oscillator. Note that the AC ground is not specified. Z1, Z2 and Z3 can be either capacitor or inductor, which can be determined later based on loop gain requirement. As mentioned above, the FET transistor can be in common-source, common-drain, or common-gate connection, which are shown in Figure 2.5.

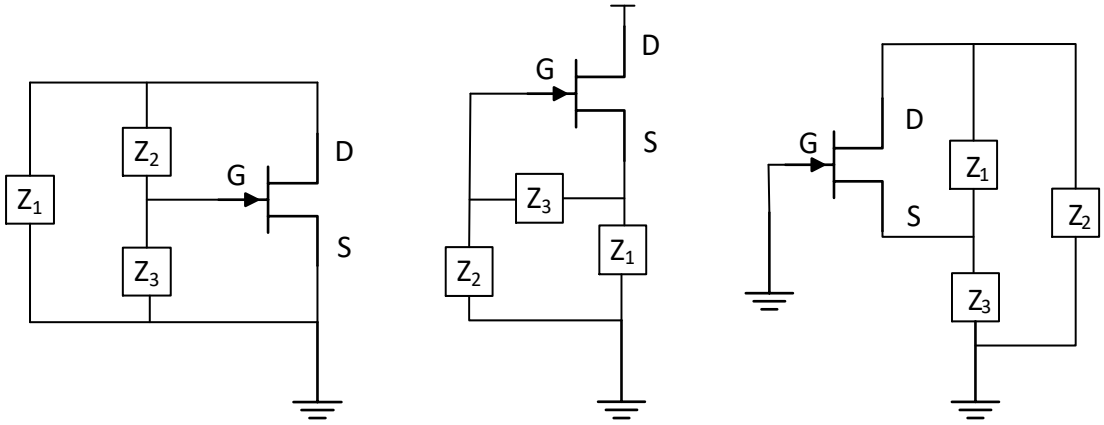

Figure 2.5 Common-source, common-drain and common-gate oscillators

2.2.1 Common Source Oscillator

Below is the small-signal circuit for common source oscillator. In feedback system point of view, it's a closed loop system. To derive the loop gain, we need to open the loop at which it has minimum load effect. Since we assume that there is no current flowing into the gate, we can just open the loop at the gate and derive the loop gain, which is the ratio of Vf to Vgs.

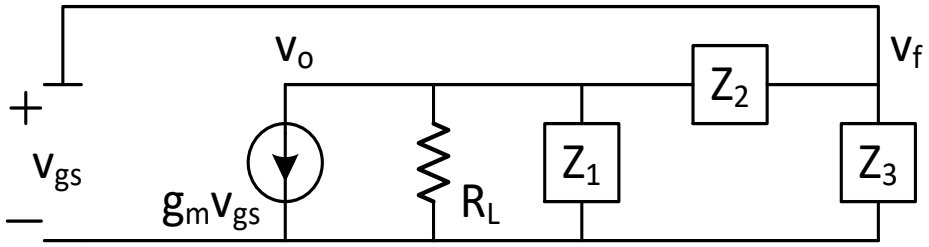

Figure 2.6 Small signal circuit of common-source oscillator

From the small-signal circuit in Figure 2.6, we can easily find that

$$\frac{V_f}{V_{gs}} = \frac{V_f}{V_o} * \frac{V_o}{V_{gs}}$$

$$= \frac{Z_3}{Z_2 + Z_3} * \frac{-g_m v_{gs} * [R_L \parallel Z_1 \parallel (Z_2 + Z_3)]}{v_{gs}}$$

$$= -\frac{Z_3}{Z_2 + Z_3} * g_m * [R_L \parallel Z_1 \parallel (Z_2 + Z_3)]$$

$$= -\frac{g_m R_L Z_1 Z_3}{R_L(Z_1 + Z_2 + Z_3) + Z_1(Z_2 + Z_3)}$$

Since Z1, Z2 and Z3 are all reactive components, we can express them as follows,

$$Z_1 = jX_1$$

$$Z_2 = jX_2$$

$$Z_3 = jX_3$$

where

$$X_i = \begin{cases} \omega L_i\,, & if\ Z_i\ is\ inductor\,; \\ -\dfrac{1}{\omega C_i}\,, & if\ Z_i\ is\ capacitor\,. \end{cases}$$

So that the loop gain can be simplified as

$$\frac{v_f}{v_{gs}} = -\frac{g_m R_L Z_1 Z_3}{R_L(Z_1 + Z_2 + Z_3) + Z_1(Z_2 + Z_3)}$$

$$= -\frac{g_m R_L jX_1 jX_3}{R_L(jX_1 + jX_2 + jX_3) + jX_1(jX_2 + jX_3)}$$

$$= \frac{g_m R_L X_1 X_3}{j(X_1 + X_2 + X_3)R_L - X_1(X_2 + X_3)}$$

Based on the Barkhausen stability criterion, we can get that

$$X_1 + X_2 + X_3 = 0$$

$$-\frac{g_m R_L X_1 X_3}{X_1(X_2+X_3)} = -\frac{g_m R_L X_3}{(X_2+X_3)} = g_m R_L \frac{X_3}{X_1} = 1$$

These are the conditions for stable oscillation. The second condition means that $\frac{X_3}{X_1}$ must be positive. That is, Z1 and Z3 must both be inductors or both be capacitors. Since $X_2 = -X_1 - X_3$, then if Z1 and Z3 are capacitors, then Z2 must be inductor, and vise verse.

Replace X_i by $\omega_o L_i$ or $-\frac{1}{\omega_o C_i}$, the frequency of oscillator and the requirement for oscillation can be determined. If Z1 and Z3 are capacitors and Z2 inductor($X_1 = -\frac{1}{\omega_o C_1}$, $X_2 = \omega_o L$, $X_3 = -\frac{1}{\omega_o C_2}$), then from

$$-\frac{1}{\omega_o C_1} + \omega_o L - \frac{1}{\omega_o C_2} = 0$$

the oscillation frequency is $\omega_o = \frac{1}{\sqrt{L*\frac{C_1 C_2}{C_1+C_2}}}$, and $g_m R_L \frac{C_1}{C_2} > 1$ is required to start the oscillation.

If Z1 and Z3 are inductors and Z2 capacitor($X_1 = \omega_o L_1$, $X_2 = -\frac{1}{\omega_o C}$, $X_3 = \omega_o L_2$), then from

$$\omega_o L_1 - \frac{1}{\omega_o C} + \omega_o L_2 = 0$$

the oscillation frequency is $\omega_o = \frac{1}{\sqrt{(L_1+L_2)*C}}$, and $g_m R_L \frac{L_2}{L_1} > 1$ is required to start the oscillation.

The topologies with specified inductor or capacitor are shown in Figure 2.7.

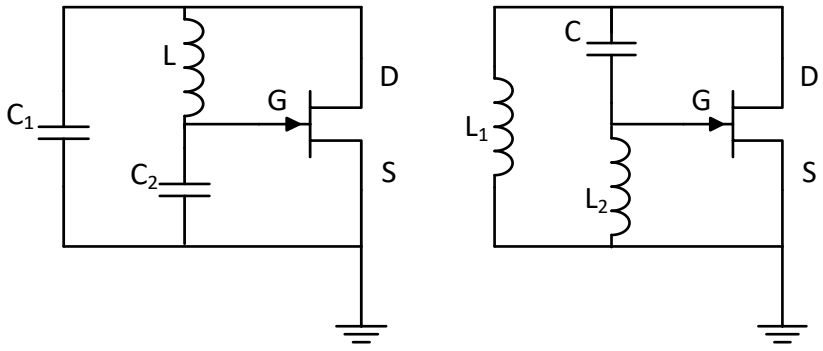

Figure 2.7 Two common-source oscillators

Notice that the dc biasing circuit is omitted in the above topologies.

Chapter 3

3 Proposed GaN-Based High Temperature VCO

3.1 High Temperature RF Transistor

The available commercial transistor for high temperature applications are limited. GaN is one of the most promising candidate for next generation power transistor, which can operate safely at extreme temperature. The commercial GaN transistors we can find when we initiate the design are from TriQuint (now Qorvo) which have an absolute channel temperature of 275 °C. Also, they are all for high power PA application. Commercial GaN transistor specialized for LNA or oscillator design is not available yet, because LNA or oscillator requires relatively low power operation and thermal issue is less a problem compared with PA. So that noise performance is not available from the datasheet. However, a number of literature shows that the noise performance of GaN device is still reasonable. The TriQuint T2G6000528-Q3 GaN transistor is one of the power transistor and then chosen based on other specifications like frequency, power, and price.

3.1.1 I-V Characterization of the transistor

I-V measurement is one of the essential part of characterization of transistor, from which device equivalent circuit model can be extracted. However, many devices have dispersion characteristics [9], which means that the measurement result is dependable on frequency. So that DC measurement may result in large inaccuracy if the device will operate at high frequency. This inaccuracy can be minimized by using pulsed measuring technique, which indicates that the

applied voltage is no longer DC. Instead, pulsed waves normally with duration less than 1 us is used to obtain I-V data for the DUT. The pulsed measuring process can be done by setting power supply which is capable of generating pulsed waves and then pulsed current data can be collected. Alternatively, there are commercially available instruments that can perform pulsed I-V measurements with options for pulse width and duty cycle [10]. In addition, data can be automatically collected and plot generated.

The measurement is carried out with DiVA D265 Dynamic I(V) Analyzer. Different ambient temperature condition is created inside the oven. The measurement results are shown in Figure 3.1~3.4 generated by I(V) tracer.

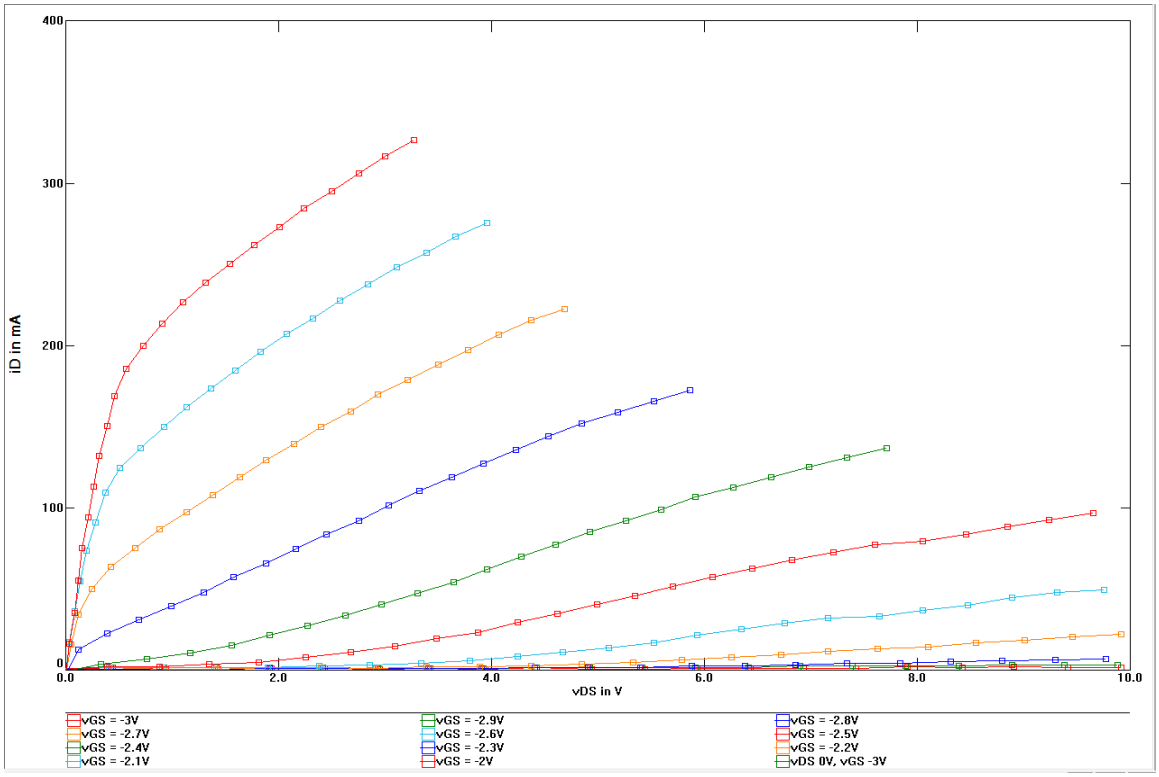

Figure 3.1 Measured I-V data of transistor at 25 °C

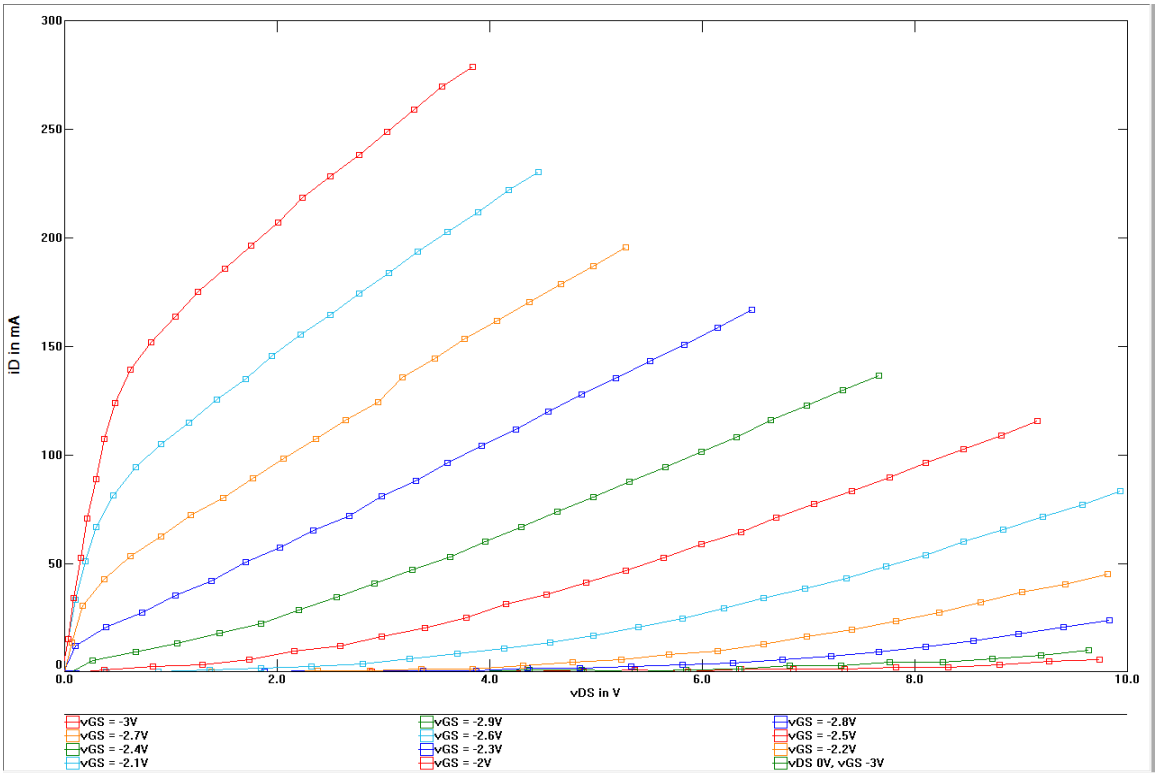

Figure 3.2 Measured I-V data of transistor at 100 °C

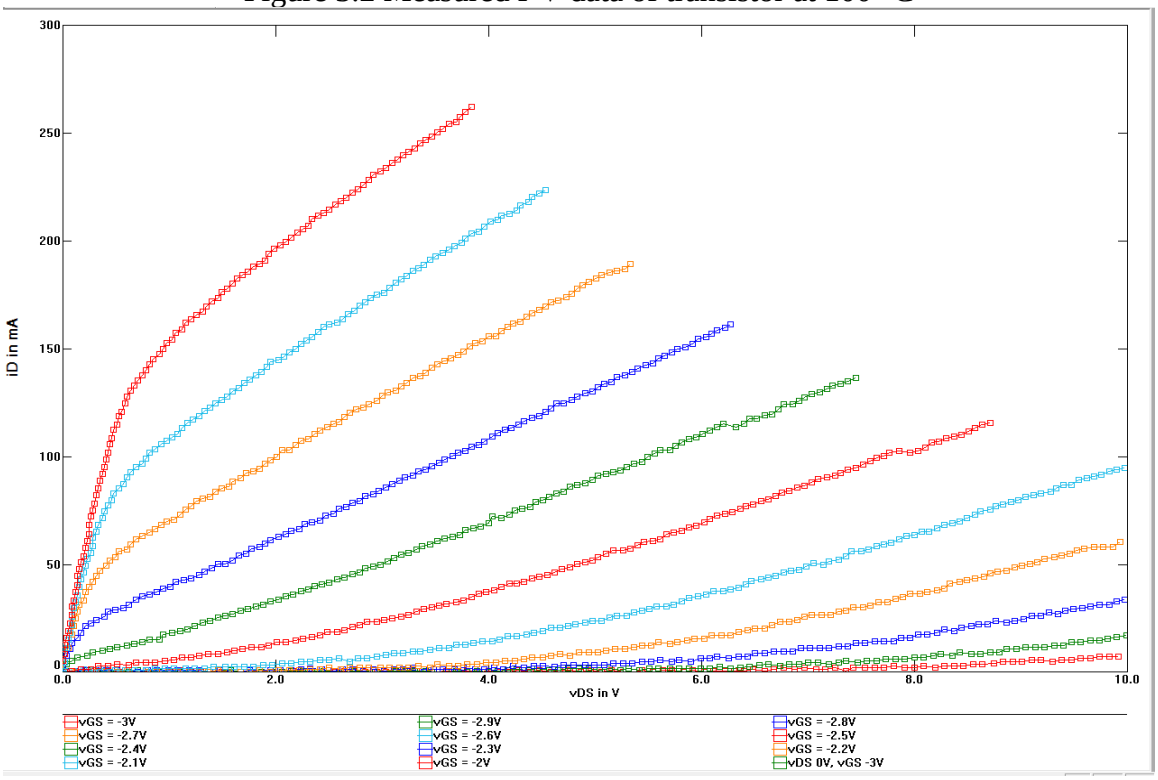

Figure 3.3 Measured I-V data at 150 °C

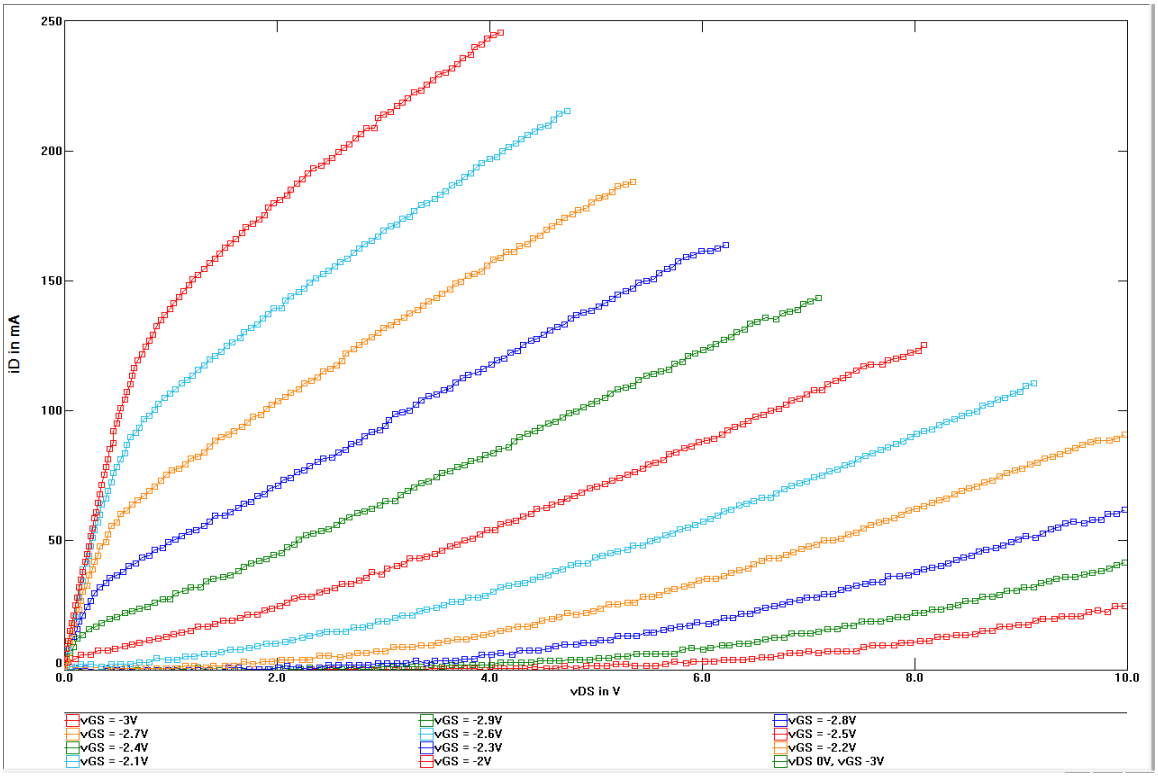

Figure 3.4 Measured I-V data at 230 °C

3.1.2 Thermal Consideration

Thermal issue is one of the most challenging problem of this design. As mentioned before, the operation ambient temperature is 230 °C and the maximum rated junction temperature is 275 °C. According to datasheet of the GaN device selected, the junction to case thermal resistance is 12.4 °C/W. The case to ambient thermal resistance is estimated to be 90.6 °C/W. So that the total thermal resistance from junction to ambient is 103 °C/W. The maximum allowable power dissipation is then

$$P_{max} = \frac{T_{J,max} - T_A}{R_T} = \frac{275 - 230}{103}\text{W} = 0.44\text{ W}$$

The actual peak power dissipation is 123 mW (see Chapter 4). So that the operating junction temperature is estimated to be

$$T_J = T_A + P_p * R_T = 230\text{ °C} + 0.123 * 103\text{ °C} = 243\text{ °C}$$

Also, the highest ambient temperature (which would result in maximum junction temperature under peak power dissipation) should be

$$T_{A,max} = T_{J,max} - P_p * R_T = 275\text{ °C} - 0.123 * 103\text{ °C} = 262\text{ °C}$$

By using an additional heatsink can further reduce the actual operating junction temperature, which can significantly increase the device lifetime, or achieve higher ambient temperature condition. However, the size and price of the circuit board will also increase.

3.2 Varactor Characterization

In addition to transistor amplifier, varactor is one of the most critical component in VCO design. Several aspects of varactor are of most interests, i.e., absolute capacity value, tuning range, quality factor and self-resonant frequency (SRF). In LC-oscillator, inductor together with capacitor and varactor compose the resonant network by which the resonant frequency is determined. So that for specific VCO operating frequency, the absolute value of varactor should be considered when determine the suitable value of inductor and capacitor. For example, one can choose value for inductor and capacitor firstly and then varactor with absolute capacity value close to the capacitor can be chosen to replace it. However, in our case, no commercial high temperature varactor is available yet. The GaN transistor is used as varactor with their source and drain terminal shorted. Then it's characterized and inductor value is determined correspondingly to make the resonator.

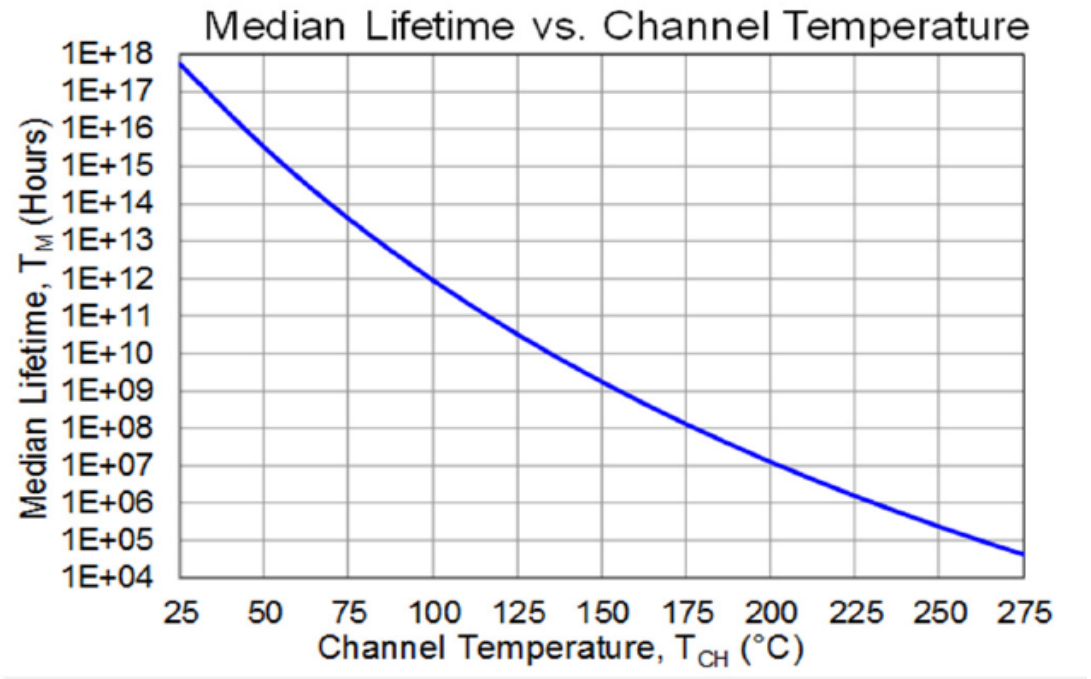

Figure 3.5 GaN transistor median lifetime as a function of channel temperature

The tuning range of the varactor can be defined by the ratio of the maximum capacitance C_{max} over minimum capacitance C_{mim} of the varactor, that is

$$TR_C = \frac{C_{max}}{C_{min}}$$

Alternatively, the tuning range can be defined using the equation

$$TR'_C = \pm\frac{1}{2}\frac{C_{max} - C_{min}}{\frac{C_{max} + C_{min}}{2}} = \pm\frac{C_{max} - C_{min}}{C_{max} + C_{min}}$$

These two definition can be related by equation

$$TR'_C = \pm\frac{TR_C - 1}{TR_C + 1}$$

The tuning range of varactor is determinant of the frequency tuning range of VCO. For example, the resonant frequency of two-element resonator with one inductor L and one capacitor C is

$$f = \frac{1}{\sqrt{LC}}$$

If capacitor C is replaced with varactor, then the maximum resonant frequency is $1/\sqrt{LC_{min}}$ and the minimum resonant frequency $1/\sqrt{LC_{max}}$. The tuning range of resonator is then

$$TR_f = \frac{f_{max} - f_{min}}{\frac{f_{max} + f_{min}}{2}} = \frac{\frac{1}{\sqrt{LC_{min}}} - \frac{1}{\sqrt{LC_{max}}}}{\frac{\frac{1}{\sqrt{LC_{min}}} + \frac{1}{\sqrt{LC_{max}}}}{2}} = \frac{\sqrt{TR_C} - 1}{\frac{\sqrt{TR_C} + 1}{2}} = 2(1 - \frac{2}{\sqrt{TR_C} + 1})$$

From the equation above, we can find that the tuning range of two-element resonator is independent of inductance and only related to the tuning range of varactor, that is, larger tuning range of varactor results in larger tuning range of resonant frequency.

(Add diagrams of the resonator)

Another very important aspect of varactor is quality factor, or Q factor. The quality factor of varactor has an effect on quality factor of resonator, which in turn can affect the noise performance of VCO. The definition of Q factor of varactor is very similar to that of a capacitor, which is defined at specific frequency by the equation

$$Q = \frac{1}{\omega C R_s}$$

where ω is the angular frequency at which Q factor is difined, C capacitance, and R_s the equivalent series resistance (ESR) of capacitor. The impedance of capacitor at ω is $Z = R_s + jX$, where $X = -\frac{1}{\omega C}$. So that the Q factor of capacitor can also be defined as

$$Q = \frac{|X|}{R_s}$$

In some cases we may find it is more convenient to represent a non-ideal capacitor with a parallel resistor and capacitor, the admittance of which is $Y = G + jB$. Since $Y = \frac{1}{Z}$, then admittance can be represented by R_s and C using equation

$$Y = \frac{\omega^2 C^2 R_s}{1 + \omega^2 C^2 R_s^2} + \frac{j\omega C}{1 + \omega^2 C^2 R_s^2}$$

Then the conductance G is equal to $\frac{\omega^2 C^2 R_s}{1+\omega^2 C^2 R_s^2}$ and susceptance $\frac{\omega C}{1+\omega^2 C^2 R_s^2}$. The Q factor can also be define by the ratio of susceptance B over conductance G as

$$\begin{aligned} Q &= \frac{B}{G} \\ &= \frac{\frac{\omega C}{1 + \omega^2 C^2 R_s^2}}{\frac{\omega^2 C^2 R}{1 + \omega^2 C^2 R_s^2}} \\ &= \frac{1}{\omega C R_s} \end{aligned}$$

It shows that no matter how we represent the parasitic of a capacitor, either with a series resistor or a parallel one, the quality factor remains unchanged. The admittance can be conveniently represented by using Q as

$$\begin{aligned} Y &= \frac{1}{R_s} \frac{\frac{1}{Q^2}}{1 + \frac{1}{Q^2}} + \frac{j\omega C}{1 + \frac{1}{Q^2}} \\ &= \frac{1}{R_s(1 + Q^2)} + j\omega C \frac{Q^2}{1 + Q^2} \\ &= \frac{1}{R_p} + j\omega C_p \end{aligned}$$

where R_p is the parallel equivalent resistor and $R_p = R_s(1 + Q^2)$, C_p the corresponding capacitance and $C_p = C\frac{Q^2}{1+Q^2}$. For $Q \gg 1$, $C_p \approx C$.

The characterization of varactor can be easily done by using a Network Analyzer. The varactor, made by grounding both source and drain terminal, is basically a one port device. Network Analyzer can be used to measure its reflection coefficient, S_{11}. The reflection coefficient can be expressed as

$$S_{11} = \frac{Z_{in} - Z_o}{Z_{in} + Z_0}$$

where Z_o is the reference impedance and chosen to be 50 ohm in most case. When S_{11} is measured, Z_{in} can also be obtained using equation

$$Z_{in} = Z_o \frac{1 + S_{11}}{1 - S_{11}}$$

If the admittance is needed, then we can just take the inverse to get

$$Y = \frac{1}{Z_o} \frac{1 - S_{11}}{1 + S_{11}}$$

The capacitance and Q factor are then

$$C = \frac{\mathrm{Im}\{Y\}}{2\pi f}$$

$$Q = \frac{\mathrm{Im}\{Y\}}{\mathrm{Re}\{Y\}}$$

The varactor is characterized at four different temperature from 25 °C to 230 °C. Figure ? shows the measurement results of capacitance. At 25 °C, it increased from 7.3 pF to 11.2 pF when the gate voltage changes from -7 V to 0V. When ambient increases, the measured capacitance decreases, with minimum of 6.7 pF and maximum of 10 pF. The Q factor is calculated based on the measured data of S_{11} and equations above. Figure ? shows the results for Q factor versus control voltage at different ambient temperature. The Q factor of varactor degrades with increasing temperature. At 25 °C, the average Q factor over different control voltage is 24.4 and it decreases to 15.0 at 230 °C.

Figure 3.6 Board for characterizing of varactor

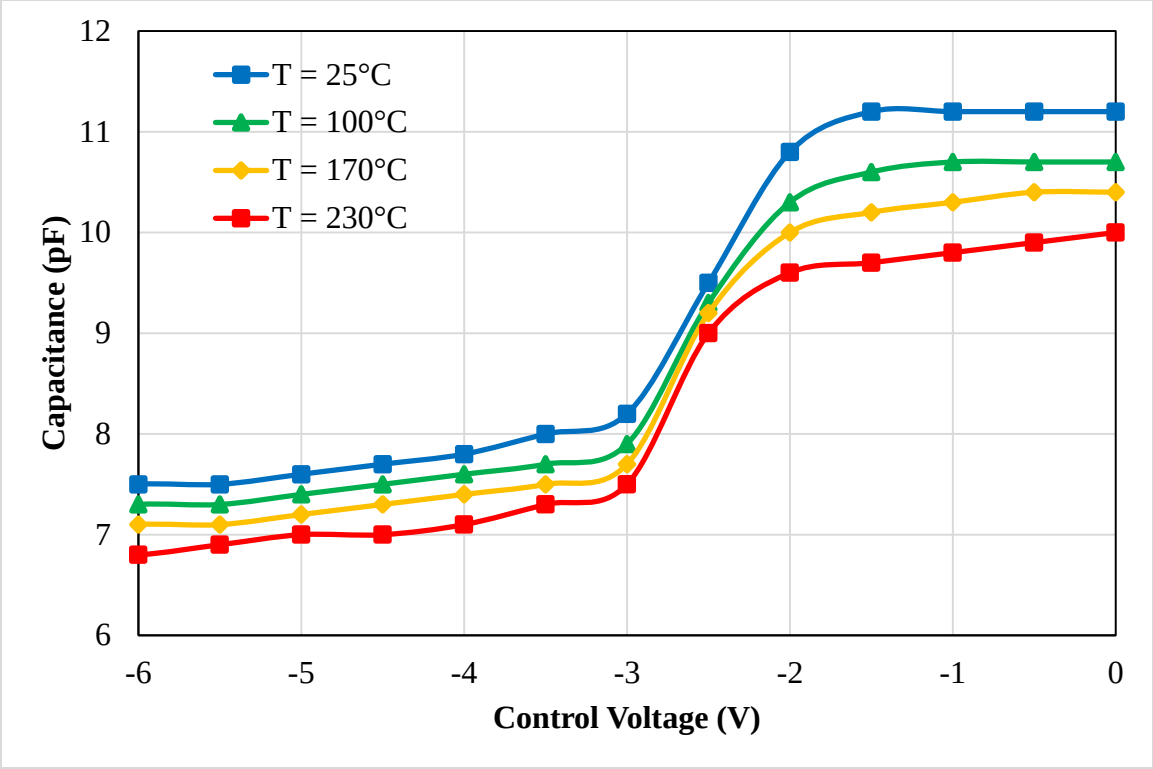

Figure 3.7 Capacitance of varactor versus control voltage at different temperatrue

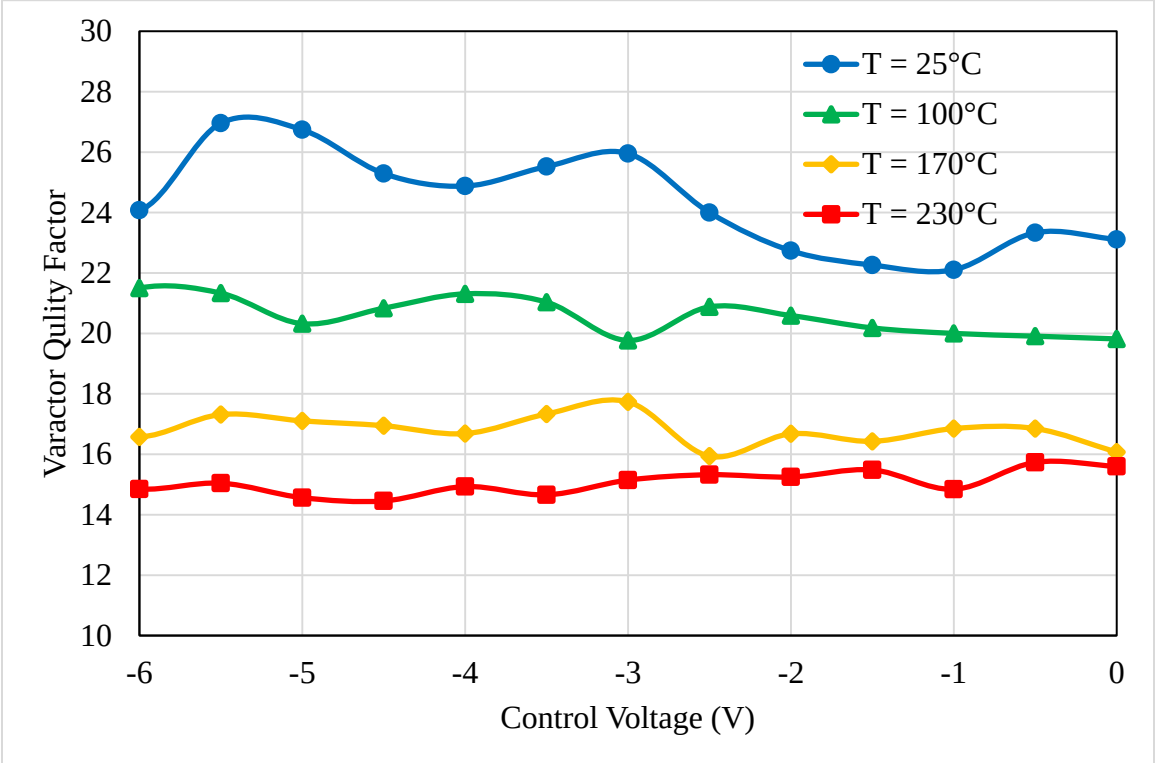

Figure 3.8 Varactor quality factor versus control voltage at different temperature

3.3 Inductor Design

Inductor is another critical part of a resonator in LC-oscillator design. Inductors can be categorized into air core inductor and ferromagnetic core inductor. In a ferromagnetic core inductor, the magnetizing field from the current carried by the coil will induce magnetization in the material, thus increasing the magnetic flux and the inductance. A high permeability ferromagnetic core can increase the inductance by a factor of several thousand. But the ferromagnetic core will also cause energy losses referred as core losses, which increase with frequency. So that, in radio frequency application, air core inductor are often selected due to its high Q factor. The exception is the RF choke (RFC), a large value inductor used to block any high frequency signal and bypass DC supply voltage.

Figure 3.9 Coilcraft AT549RBT extreme temperature inductor [fair use]

In this design, Coilcraft extreme temperature coil AT549RBT is selected as the RFC, which is designed for use in high-temperature applications up to 300 °C. The specification is listed in the table below.

Table 3-1 Specification of Coilcraft AT549RBT inductor [fair use]

Part Number	Inductance ±20% (μH)	DCR max (mΩ)	SRF min (MHz)	Imax (A)
AT549RBT102MLZ	1.0	15.0	800	1.0

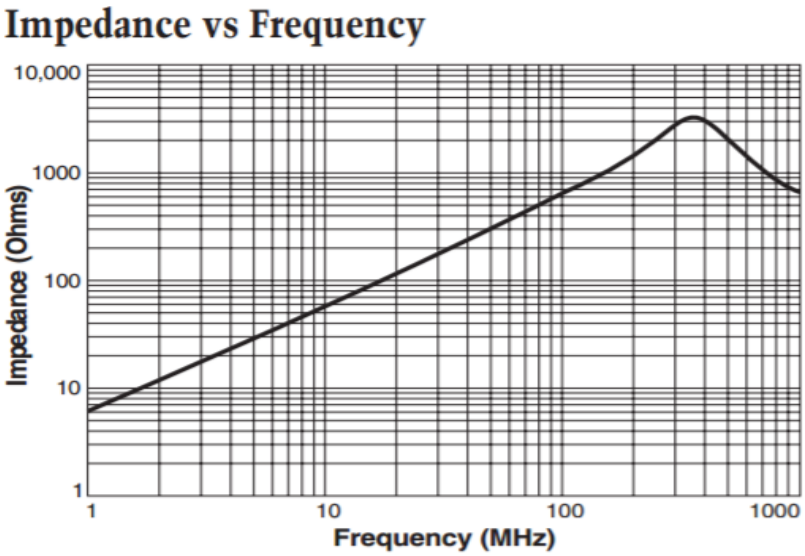

Figure 3.10 AT549RBT inductor impedance v.s. frequency [fair use]

It can be seen from the figure above that the impedance of the coil is around 3 KΩ at frequency near 340 MHz, which is much larger than the impedance seen from the gate of the transistor and from the source.

Air-core inductor is selected in the resonator part in our design due to its high quality factor. During the design, rough value of inductor is determined based on circuit simulation and then several types of inductors, with different diameters of coil, diameters of wire, and number of turns, are made and tested to find the suitable structure.

There are also a number of ways to calculate the inductance of air-core coil developed by different physicists, among which the most famous one is

$$L = \frac{1}{l}\mu_0 N^2 A$$

where l is the length of coil, μ_0 the permeability of free space, N the number of turns and A the area of cross-section of coil, all in SI units.

Generally, these formulas are derived under certain assumptions and must be applied with restrictions. H. Nagaoka [11] tabulated a certain coefficient (which is dependent on the length of coil and was later referred as Nagaoka coefficient) such that the self-inductance of a solenoid, no matter long or short, can be calculated easily. However, this work is under a common supposition of a cylindrical current sheet and the thickness of the wire and insulation layer is not taken into account. Edward B. Rosa's work take into account both the length of coil and thickness of wire. However, the shape of the wire is ignored and assumed to be square. In D. Knight's work [12], the

thickness and shape of the inductor are both taken into account. The diameter of the coil is replaced with the so called effective current-sheet diameter. At low frequency,

$$D_0 = D_a\left[1 - \left(\frac{d}{D_a}\right)^2\right]$$

where D_0 is the equivalent current-sheet diameter at low frequency, d the diameter of round wire and D_a the average diameter of the helix. At high frequency, skin effect and proximity effect must be considered, which cause the effective current-sheet diameter at high frequency (denoted as D_∞) hard to be determined. However, the absolute minimum value can be found, which is

$$D_{min} = \frac{[(N-2)(D_a - d) + 2D_0]}{N}$$

Then a semi-empirical formula for D_∞ can be defined to be

$$D_\infty = \frac{D_0 + D_{min}\frac{a}{\frac{p}{d} - 1}}{1 + \frac{a}{\frac{p}{d} - 1}}$$

where $\frac{p}{d}$ is the pitch ratio and a purely a empirical coefficient and set to 2.

The measurement of inductance is also carried out with a Network Analyzer. The two port s-parameters of inductor are taken so than the impedance of the inductor with a series reference resistance of 50 Ω can be obtained from measured s_{11} or s_{22} as

$$Z = Z_0\frac{1 + s_{11}}{1 - s_{11}}$$

Then the inductance can be derived from the equation below.

$$L = \frac{\mathrm{Im}\{Z\}}{2\pi f}$$

Seven solenoids are made to test, all with the same wire and diameter of coil.

Table 3-2 Size of inductors for test

N	2	3	4	5	6	7	8
d (mm)	1.024						
D_1 (mm)	2.053						
L (nH)	11.8	16.7	21.3	26.0	32.7	37.2	42.0

When number of turns is small, the inductance is much smaller than that expected by the equation. This is due to because the ignorance of Nagaoka coefficient, which is much smaller than one when the number of turns of the solenoid is small.

The conductance of copper is $5.96 * 10^7$ S/m. So that the DC resistance of the inductor can be found by equation below.

$$R_{DC} = \frac{l_c}{\sigma A}$$

where $A = \frac{\pi d^2}{4}$ is the cross-section of the copper wire, $l_c = N * \pi D_a$ the length of copper wire and σ the conductivity of copper. Due to skin effect, the resistance of a straight copper wire with the same length is

$$R_{AC} = R_{DC} \frac{d}{4\delta}$$

where $\delta = \frac{1}{\sqrt{\pi f \mu \sigma}}$ is the skin depth and $\delta = \frac{0.066}{\sqrt{f}}$ m for coper. In our design frequency range of interest, the skin depth at 340.5 MHz is then $3.58*10^{-6}$ m. In addition, proximity effect [13] should also be considered for solenoid with turns larger than 1. The equation for resistance after consideration of proximity effect is then modified to be

$$R_M = \phi_M R_{AC}$$

R_M is referred as Medhurst resistance. ϕ_M is an experimental coefficient and can be found in the table below.

	ℓ_w/D						
d/z_1	1	2	4	6	8	10	∞
1	5.55	4.10	3.54	3.31	3.20	3.23	3.41
0.9	4.10	3.36	3.05	2.92	2.90	2.93	3.11
0.8	3.17	2.74	2.60	2.60	2.62	2.65	2.81
0.7	2.47	2.32	2.27	2.29	2.34	2.37	2.51
0.6	1.94	1.98	2.01	2.03	2.08	2.10	2.22
0.5	1.67	1.74	1.78	1.80	1.81	1.83	1.93
0.4	1.45	1.50	1.54	1.56	1.57	1.58	1.65
0.3	1.24	1.28	1.32	1.34	1.34	1.35	1.40

Figure 3.11 ϕ_M value of different size of coil

Take the 7-turn inductor as an example. The DC resistance is then

$$R_{DC} = \frac{l_c}{\sigma A} = \frac{N * \pi D_a}{\frac{\pi d^2}{4}\sigma} = \frac{4ND_a}{d^2\sigma} = 0.0014\ \Omega$$

AC resistance is

$$R_{AC} = R_{DC}\frac{d}{4\delta} = 0.0987\ \Omega$$

Considering proximity effect, referring to table above, $\frac{d}{z_1} = 1$ & $\frac{l_w}{D} = 2.32$, so that we can get ϕ_M close to 4.10.

$$R_M = \phi_M R_{AC} = 0.405\ \Omega$$

At 340.5 MHz, the quality factor of the inductance is roughly

$$Q = \frac{\omega L}{R_M} = 180$$

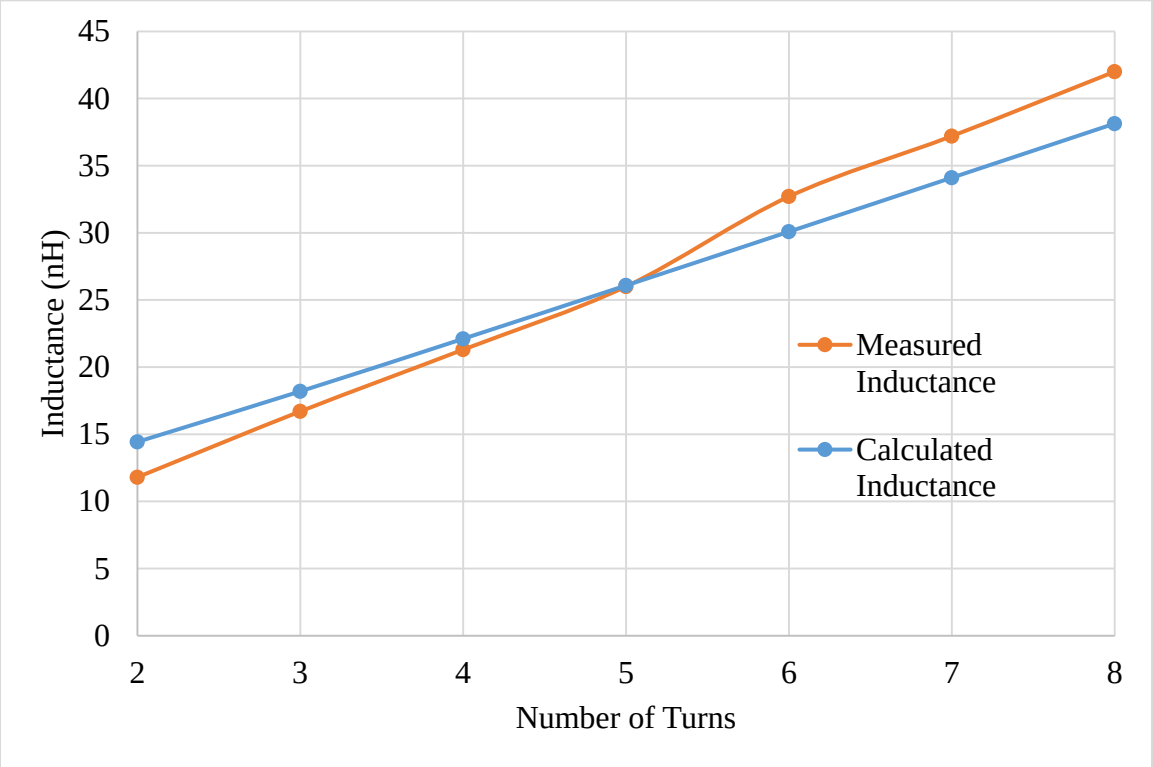

Figure 3.12 Inductance of air-core inductor base on measurement and calculation

After the entire VCO board is made, the inductor can be adjusted to make the VCO operating at pre-specified frequency range.

3.4 Proposed VCO Topology and Simulation Result

The VCO topology is shown in Figure 3.13. It can be easily found that it is based on the common-source Collipitts oscillator topology with two capacitors replaced with two identical varactors. The benefit is that both large tuning range of frequency flat output power can be achieved.

The simulation of the circuit is carried out in ADS (Advanced Design Software) software. The circuit for simulation in ADS is shown in Figure 3.14. As shown in the figure, transistor in the amplifier block is biased with V_{GS} equal to -2.5 V and V_{DS} equal to 2.5 V. The inductor in the LC tank is 65 nH, which is modified in the real board to obtain right frequency since the inaccuracy of the transistor model in simulation. Two varactors are biased with same voltage. In Figure 3.15, simulation of loop gain is plotted in polar form. The bias for varactors is -3 V. It shows that at 350.4 MHz, the phase of loop gain is zero and magnitude is larger than 1, which indicates the potential to oscillator at 350.4 MHz. The oscillation frequency can be tuned by changing the bias voltage of varactors.

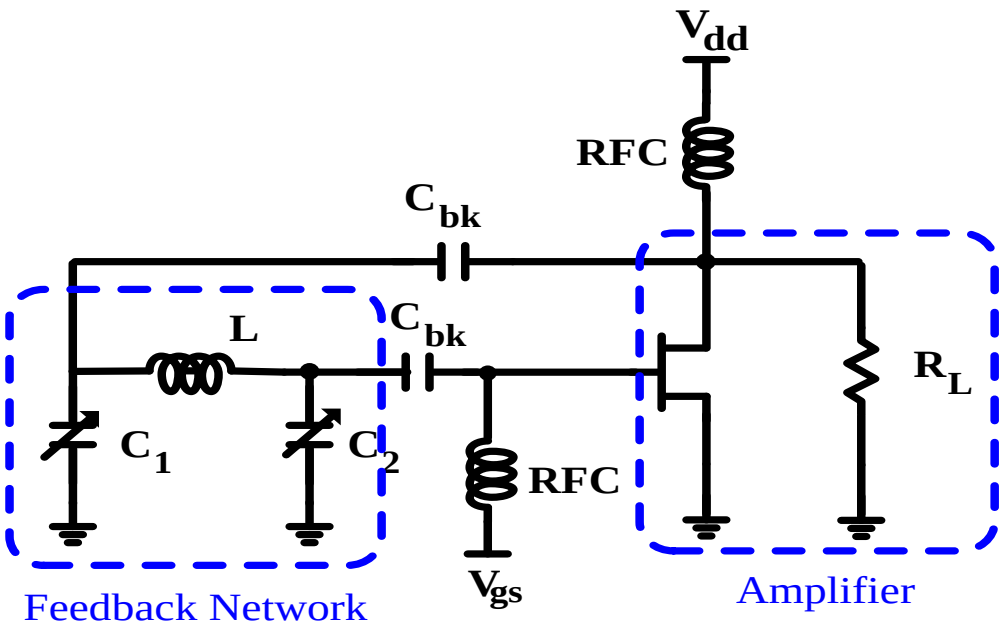

Figure 3.13 Proposed VCO topology with two balanced varactor

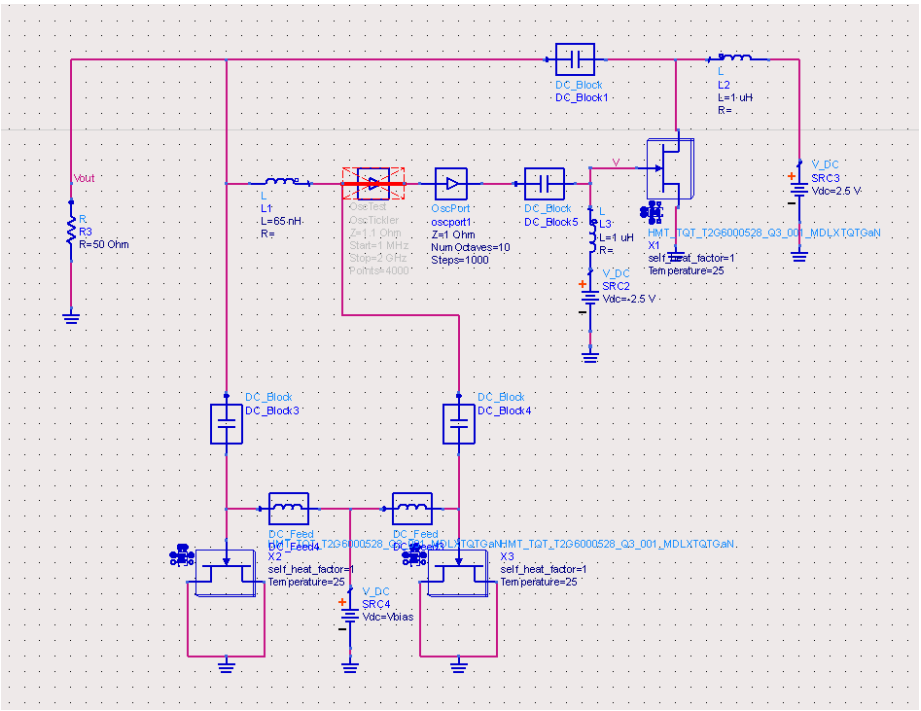

Figure 3.14 VCO Circuit for simulation in ADS

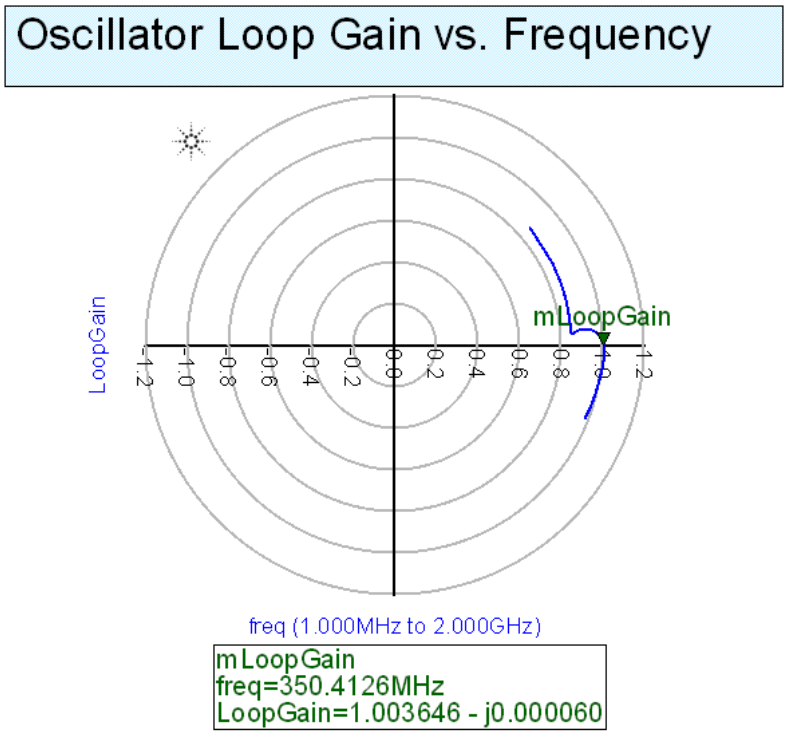

Figure 3.15 Simulation of loop gain

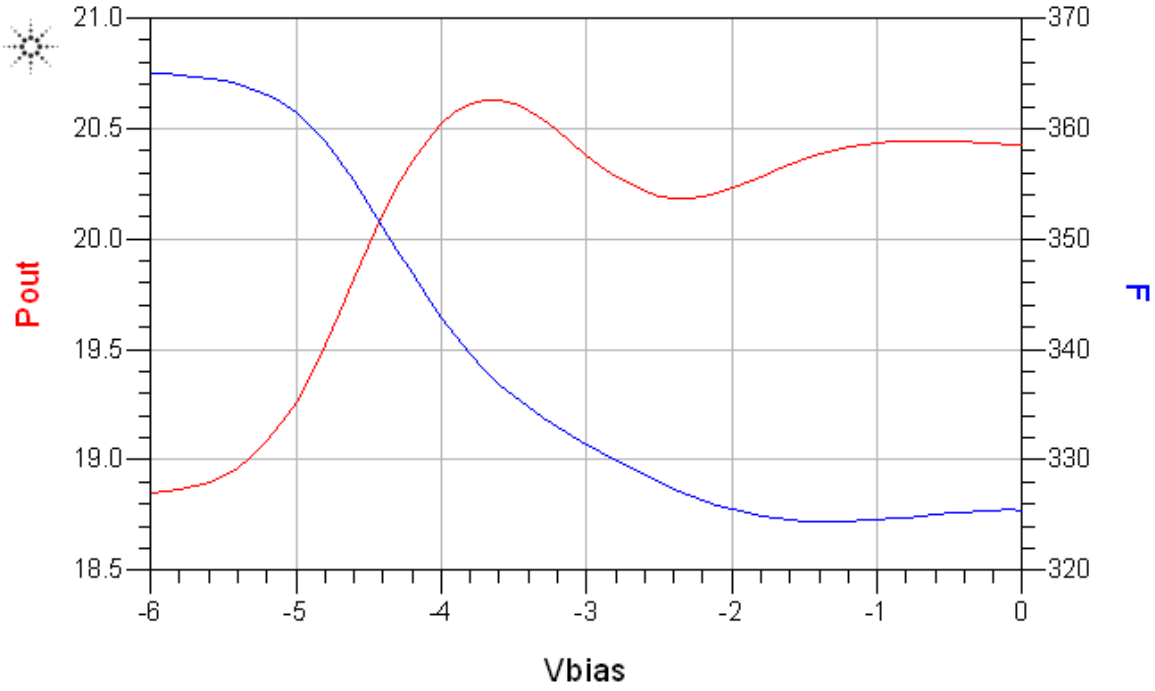

Figure 3.16 Simulation operating frequency and output power v.s. bias voltage of varactors

Performance of VCO can be simulated using Harmonic Balance technique which is incorporated in ADS software. The simulated operating frequency and output power is shown in Figure 3.16. The operating freuqncy is from 324.4 MHz to 365.1 MHz, which indicates a tuning range of 40.7 MHz. The output power is from 18.8 dBm to 20.6 dBm and the variation is 1.8 dB.

3.5 VCO Prototype

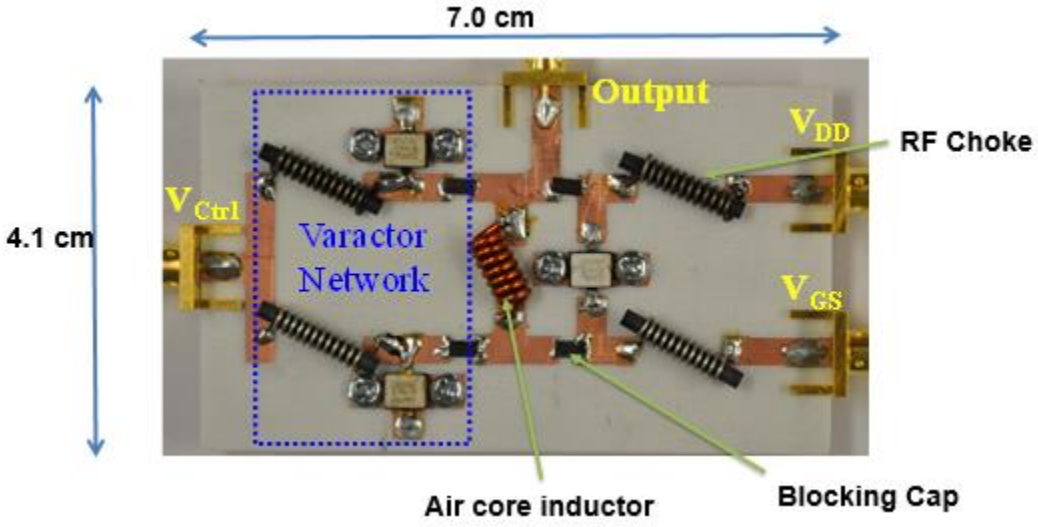

Figure 3.17 Prototype of high temperature VCO

The VCO is fabricated on Rogers 4003-RF/Microwave PCB material and the board is made using LPKF milling machine. The air-core inductor is tuned base on measurement result of the board to achieve right operating frequency range.

Chapter 4

4 Measurement Results

4.1 Measurement Instruments

4.1.1 Spectrum Analyzer

The basic performance metrics of VCO are operating frequency, output power, phase noise and harmonic distortion. The Spectrum Analyzer is the main instrument from which we can obtain the performance of VCO, like operating frequency, output power, harmonic distortion and phase noise.

4.1.2 Power Supply

RIGOL DP832A Power Supply is used to provide DC biasing of the oscillator and also the control voltage of the varactor. The Power Supply has three channels, two of which are capable of 0 to 30V/0 to 3A output Voltage/Current, and the third one is capable of 0 to 5V/0 to 3A. The OVP/OCP (Over-Voltage-Protection/Over-Current-Protection) are 1mV to 33V/1ma to 3.3A and 1mV to 5.5V/1mA to 3.3A, correspondingly. The Load and Linear Regulation Rate(Output Percentage + Offset) are both within +- (0.01%+2mV). For the biasing for VCO, the accuracy should be around… The Normal Mode Voltage ripples and noise is less than 350uVrms/2mVpp. (two values are not consistent? 350u*sqrat(2)*2=1m) from 20Hz to 20MHz. Is this the reason why we observed the spike at approximately 1MHz offset when measured the Phase Noise? In our case, the GaN device need negative gate biasing and control voltage for varactor. We can simply flip the adapter (Double Banana Plug to 50 Ohm BNC Adapter) to get negative voltage.

Figure 4.1 Rigol DP832A Power Supply [fair use]

4.1.3 Network Analyzer

The importance of a Network Analyzer can never be overestimated in RF device characterization and performance measurement, which simply stems from the importance of s-parameters in RF and Microwave circuit design. The difference of measurement of s-parameters from z or y parameters is the chosen of termination. For s-parameter measurement, 50 ohm purely resistive termination is required, instead of short-circuity or open-circuity, which are both extreme condition and hard to obtain over certain frequency. 50 ohm termination simply avoid this rigid requirement. However, there is still imperfection of test hardware and calibration will be needed every time before measurement to remove the systematic errors, the largest contributor to measurement uncertainty.

In our frequency of interest, SMA launch port and coaxial cable are used to assemble the board and connected to instrument. So that the SLOT (Short-Load-Open-Through) calibration procedure is most suitable and simple to conduct. The built-in port-extension function can de-embed the effect of microstrip line between the DUT and Ports of board from measurement result.

4.1.4 Oven

We use the oven to create the high temperature environment. The maximum operating temperature is 300 C which is well beyond our specification. The temperature control accuracy is +-1.0C at 300C, while the temperature uniformity is +-10C at 300C.

4.2 Measurement Results

The operating temperature of interest is at 230 C, which is well above room temperature. Measurement are taken at two intermediate temperatures at 100C and 170C, in addition to 25C and 230C. As mentioned before, the high temperature environment is created by the oven, which unavoidably had a temperature non-uniformity of about +-10C. At each temperature, the biasing Drain and Gate voltages remain the same. The control voltage of varactors are tuned to change the operating frequency, along with which fundamental signal power and its harmonics power, different drain current, power consumption and phase noise at 100KHz and 1MHz offset are recorded.

4.2.1 Measurement at 25 °C

The oscillator is biased with V_{DS} of 2.5V and V_{GS} of -2.5V. The control voltage varies from -6V to 0V and maximum frequency tuning range can be obtained. The frequency decreases from maximum value of 367.7MHz to 327.5 MHz when the control voltage of varactors increases from -6V to 0V. The tuning range is 40.2MHz. The output power varies in the range from 18.16dBm to 18.99dBm, which means a variation of 0.83dB in band. The second harmonic is over 20dB blow the fundamental signal. Even though the third harmonic is only 12~13dB less than fundamental signal, since its further apart from the fundamental signal that second harmonic, it's much easier to be filtered out, which results in more balanced performance of harmonics rejection. The Phase Noise of the VCO at 100KHz offset ranges from -119dBc/Hz to -131dBc/Hz. At 1MHz offset, it is in the range of -139dBc/Hz to -151dBc/Hz, a reduction of about 20dB observed.

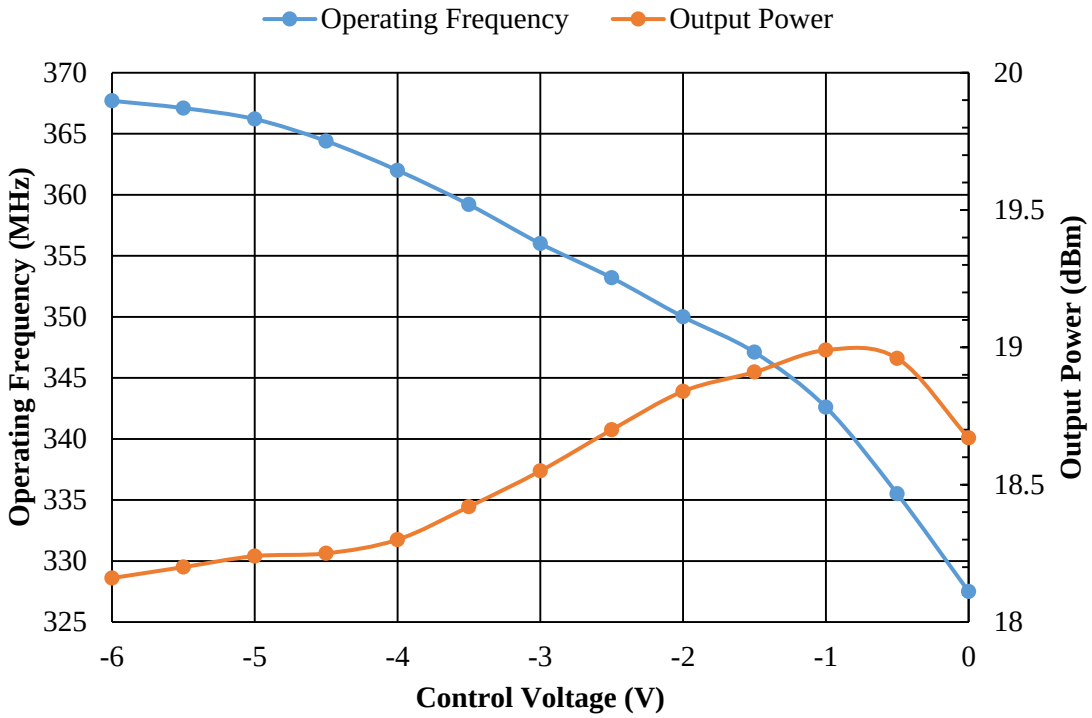

Figure 4.2 VCO operating frequency and output power versus control voltage at 25 °C

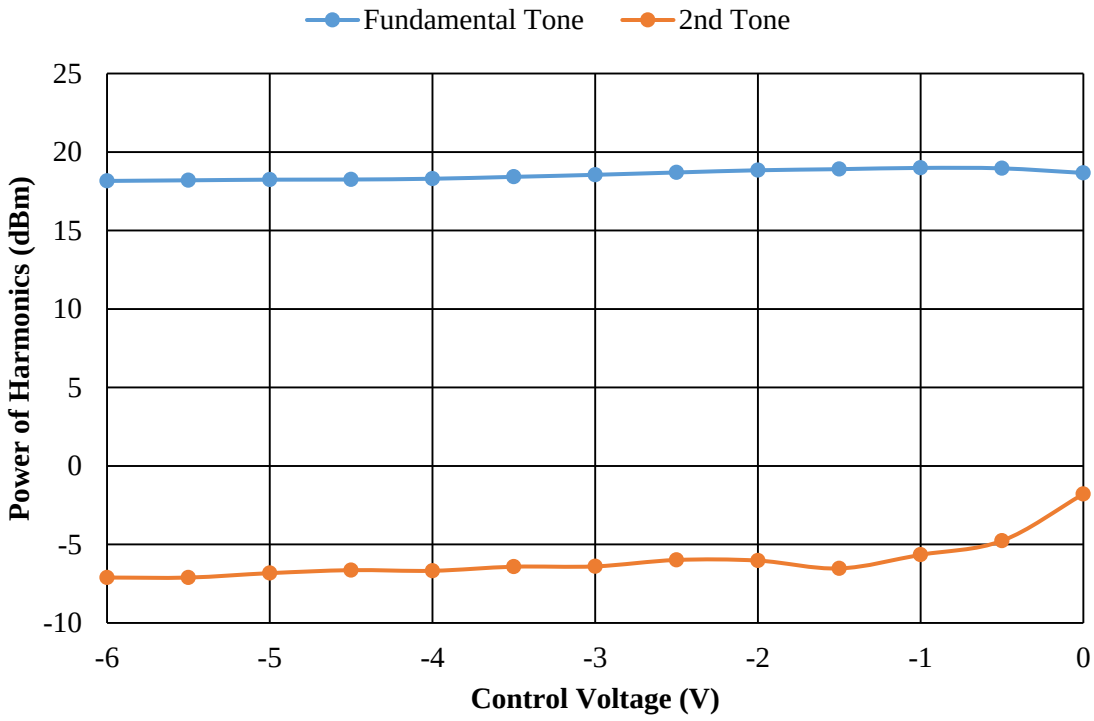

Figure 4.3 Fundamental power and second harmonic versus control voltage at 25 °C

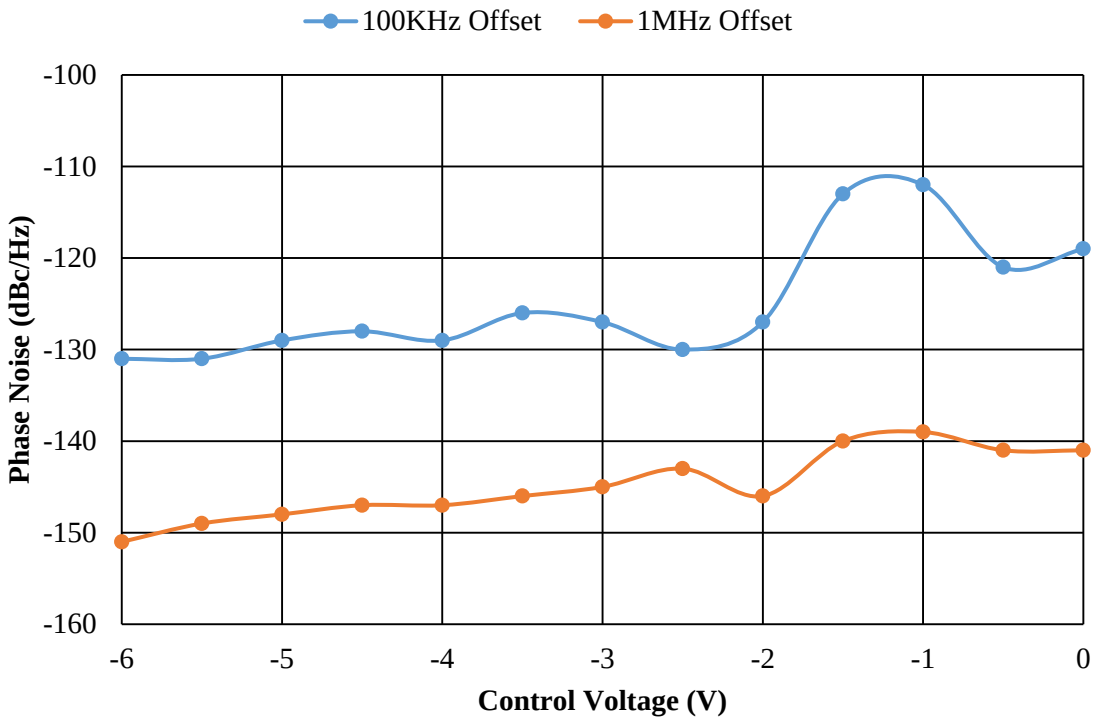

Figure 4.4 Phase noise at 100 KHz and 1 MHz offset at 25 °C

4.2.2 Measurement at 100 °C

In order to measure the performance of VCO at 100C, the oven, with the VCO board inside, is set to 100C. It takes roughly half hour to reach this temperature and extra 2~3 minutes to settle down. The performance of VCO varies with a similar trend as at room temperature, even though absolute changes occurs as expected. For operating frequency, it now ranges from 365.6MHz to 325.2MHz, which means a tuning range of 40.4MHz. The tuning range increases few, by 0.2MHz, while the absolute frequency range goes down by around 2MHz. The output power is from 17.73 dBm to 18.40 dBm, which means variation of 0.67 dB. Phase noise at 100 KHz offset is from -129 dBc/Hz to -111 dBc/Hz and at 1 MHz from -150 dBc/Hz to -140 dBc/Hz. Second harmonic is around -28.4 dB ~ -20.72 dB below fundamental signal. Third harmonic is much higher than second harmonic and around -13.18 dB ~ -12.55 dB below fundamental signal.

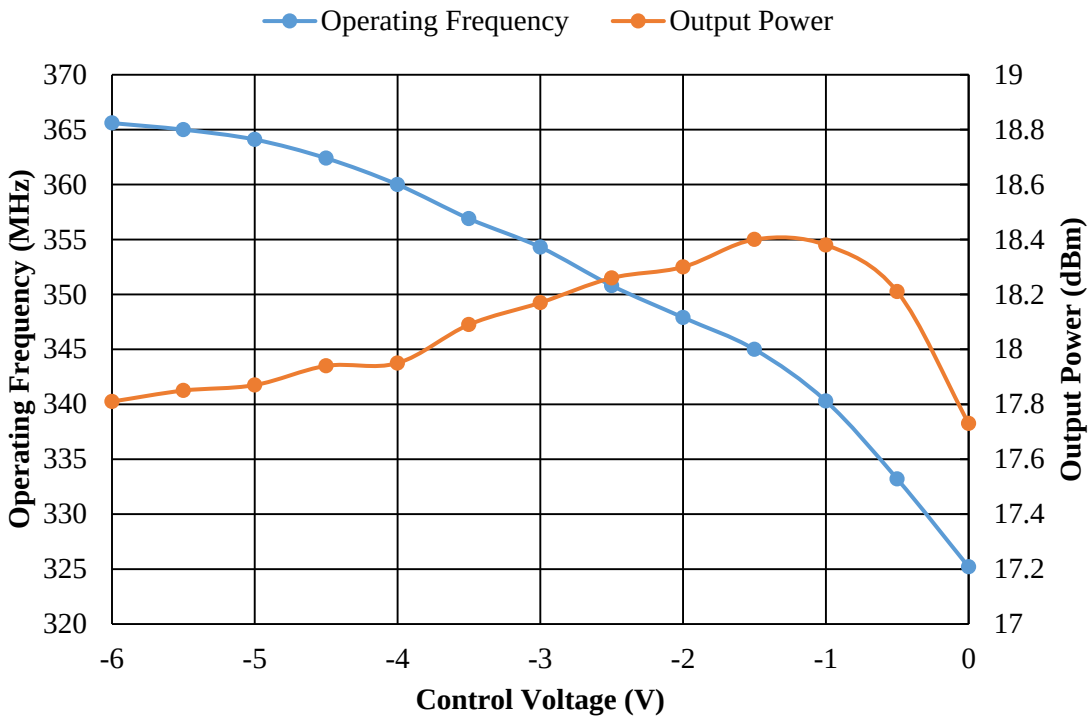

Figure 4.5 Operating frequency and output power versus control voltage at 100 °C

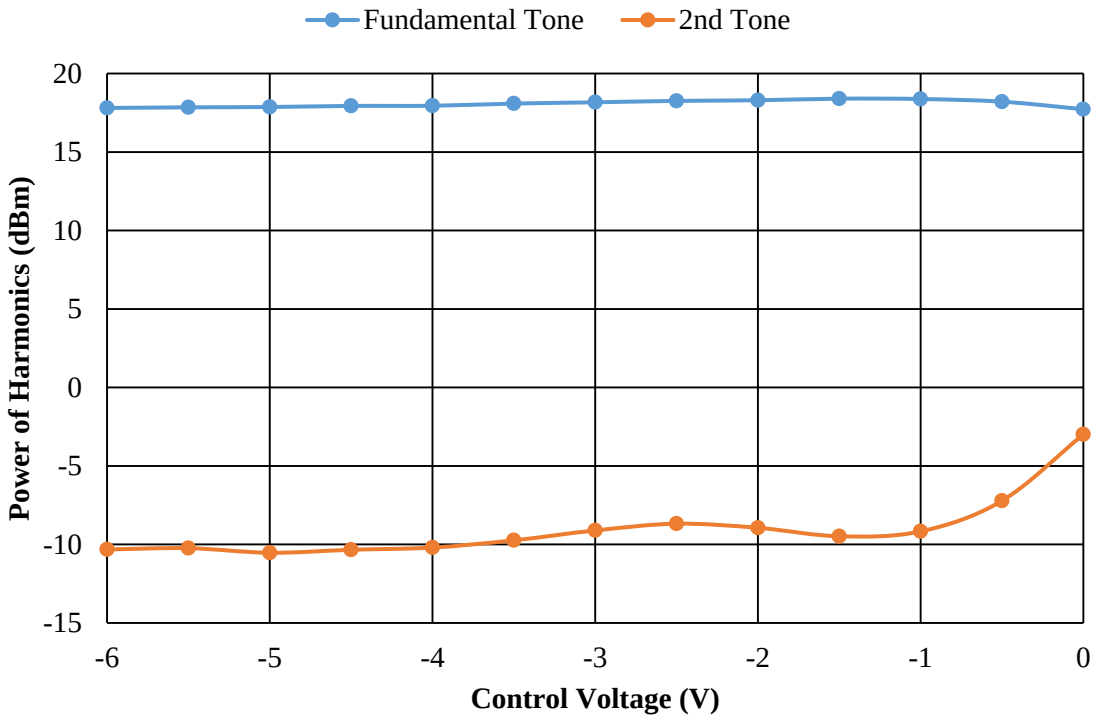

Figure 4.6 Power of fundamental tone and second harmonic at 100 °C

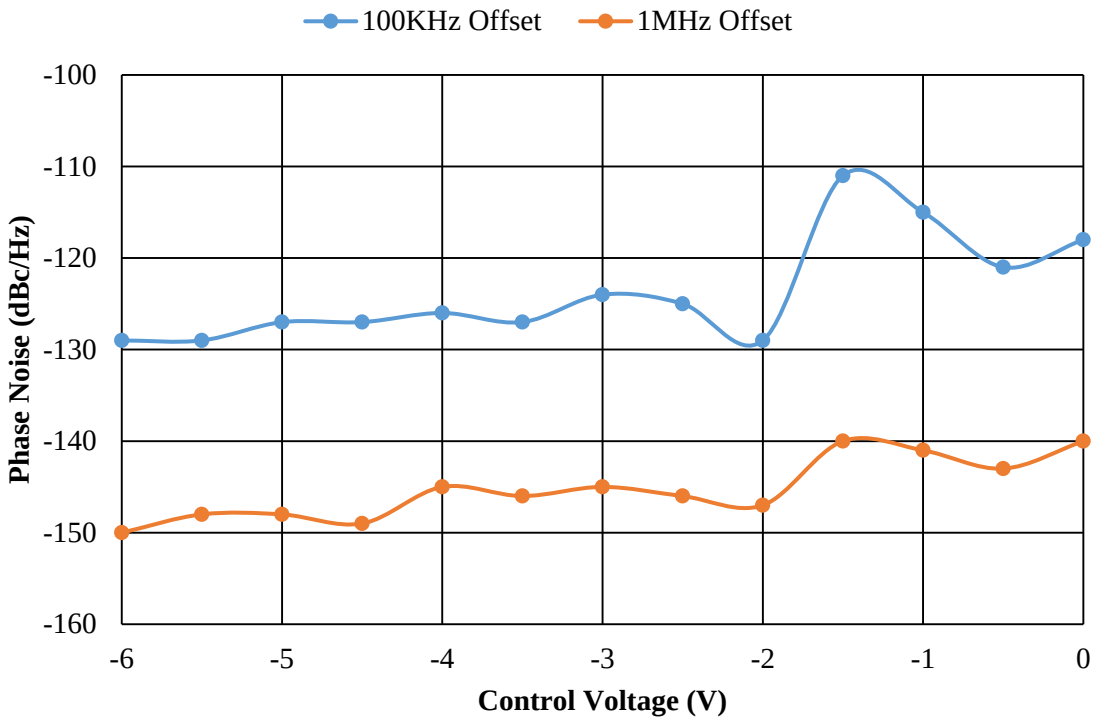

Figure 4.7 Phase noise at 100 KHz and 1MHz offset at 100 °C

4.2.3 Measurement at 170 °C

Again, the same biasing is used, namely 2.5 V for V_{DS} and -2.5 V for V_{GS}. The operating frequency is now from 322.9 MHz to 363 MHz. The tuning range is 40.1 MHz. The output power with a high of 18.17 dBm and low of 17.43 dBm. The variation is then 0.74 dBm. The highest second harmonic is -5.02 dBm, -22.45 dB below corresponding fundamental signal and the lowest harmonics is -18.33 dBm, -36.09 dB below fundamental signal. The third harmonic is from 4.1 dBm to 5.53 dBm and -13.33 dB to -12.64 dB below fundamental signal. The phase noise at 100 KHz offset is from -123 dBc/Hz to -109 dBc/Hz and at 1 MHz offset from -148 dBc/Hz to -140 dBc/Hz.

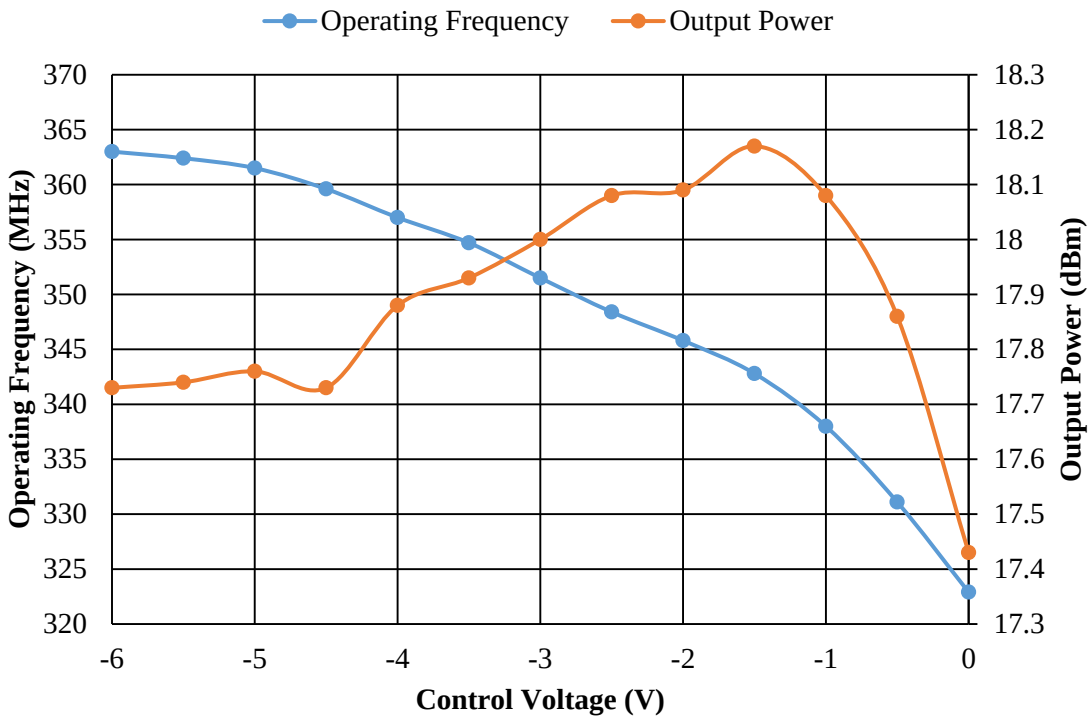

Figure 4.8 Operating frequency and output power of VCO versus control voltage at 170 °C

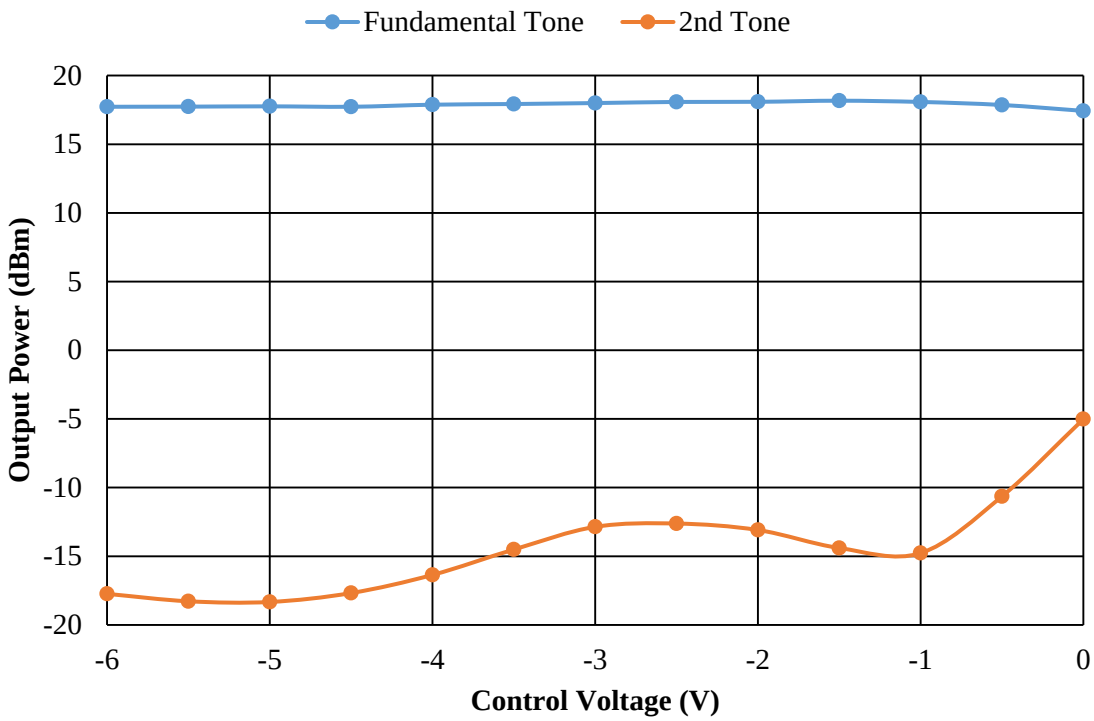

Figure 4.9 Power of fundamental tone and second harmonic at 170 °C

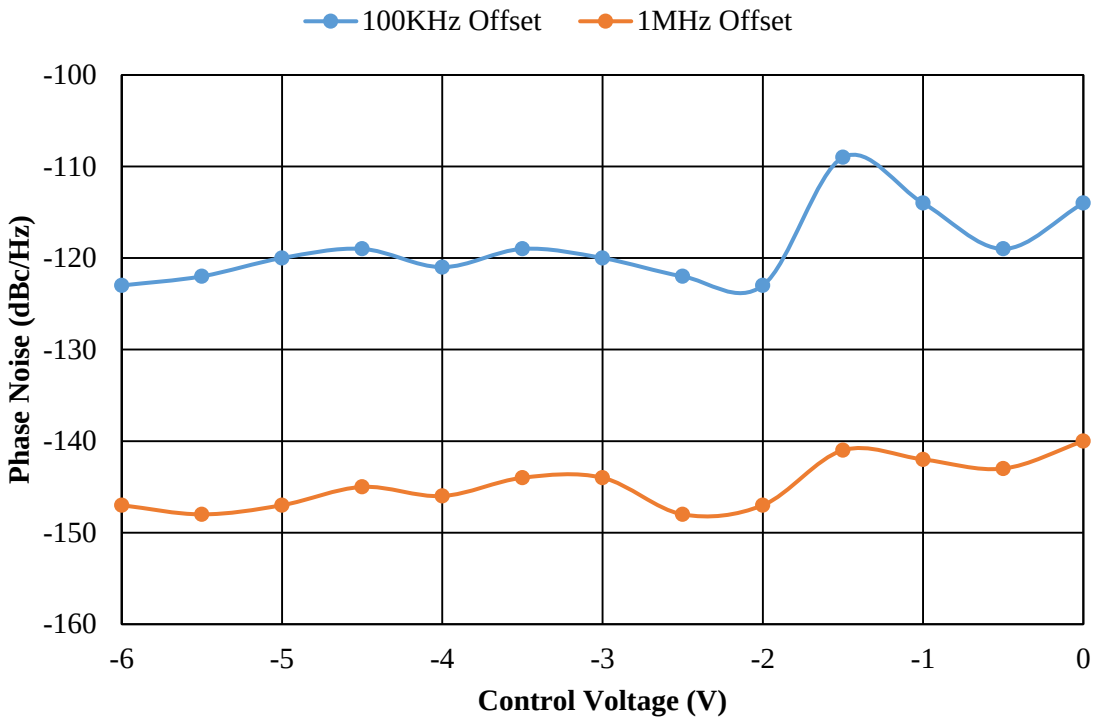

Figure 4.10 Phase noise at 100 KHz and 1 MHz offset at 170 °C

4.2.4 Measurement at 230 °C

At 230 °C, the VCO board is still biased with Vds of 2.5 V and Vgs of -2.5 V. 230 °C is our target operating temperature and is most close to the maximum rating junction temperature of the transistor. When the control voltage is tuned from -6 V to 0 V, the highest drain current is 49 mA and lowest 43 mA. The highest power consumption is the 122.5 mW. The operating frequency is from 320.8 MHz to 360.2 MHz at 230 °C. Highest output power is 17.96 dBm and lowest 17.11 dBm, which shows variation of 0.85 dBm. The second harmonic is from -31.25 dBm to -7.79 dBm, which is -48.93 dB to -24.9 dB below fundamental signal. The third harmonic is much higher than second harmonic and it's from 3.48 dBm to 5.2 dBm, which is -13.63 dB to -12.69 dB below fundamental signal. The phase noise at 100 KHz is in the range of -121 dBc/Hz to -109 dBc/Hz and at 1 MHz offset is from -146 dBc/Hz to -137 dBc/Hz.

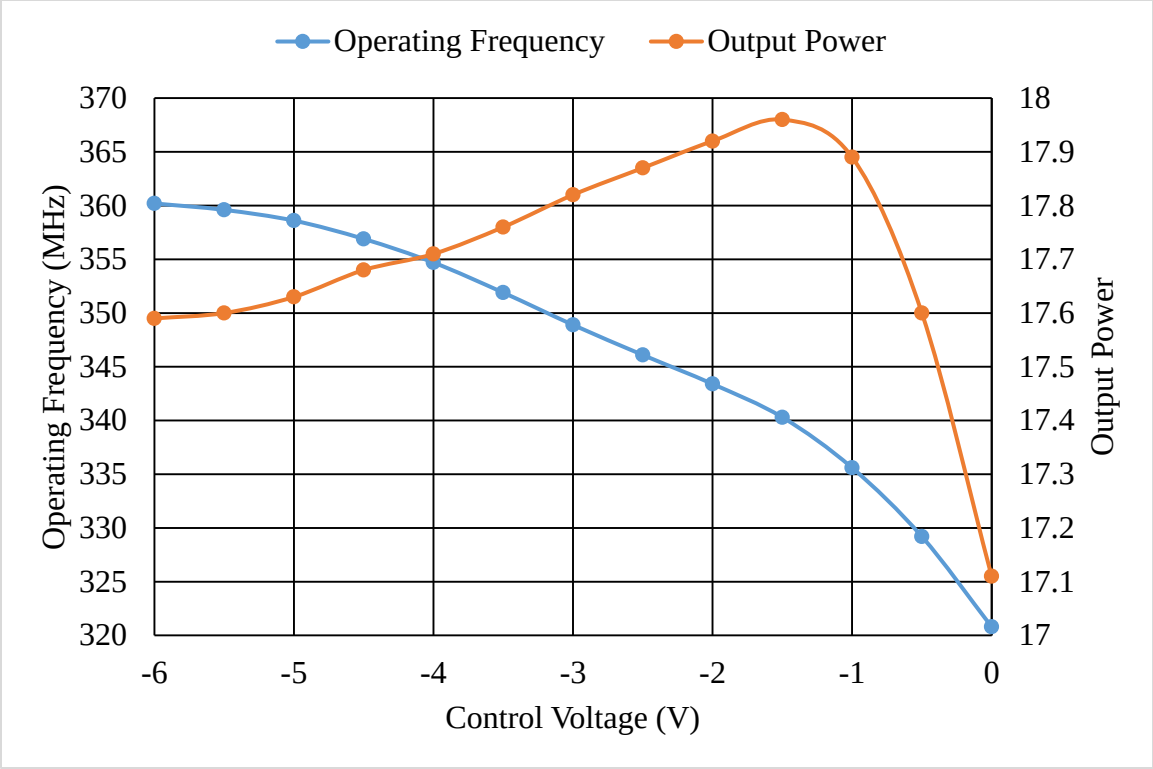

Figure 4.11 VCO operating frequency and output power versus control voltage at 230 °C

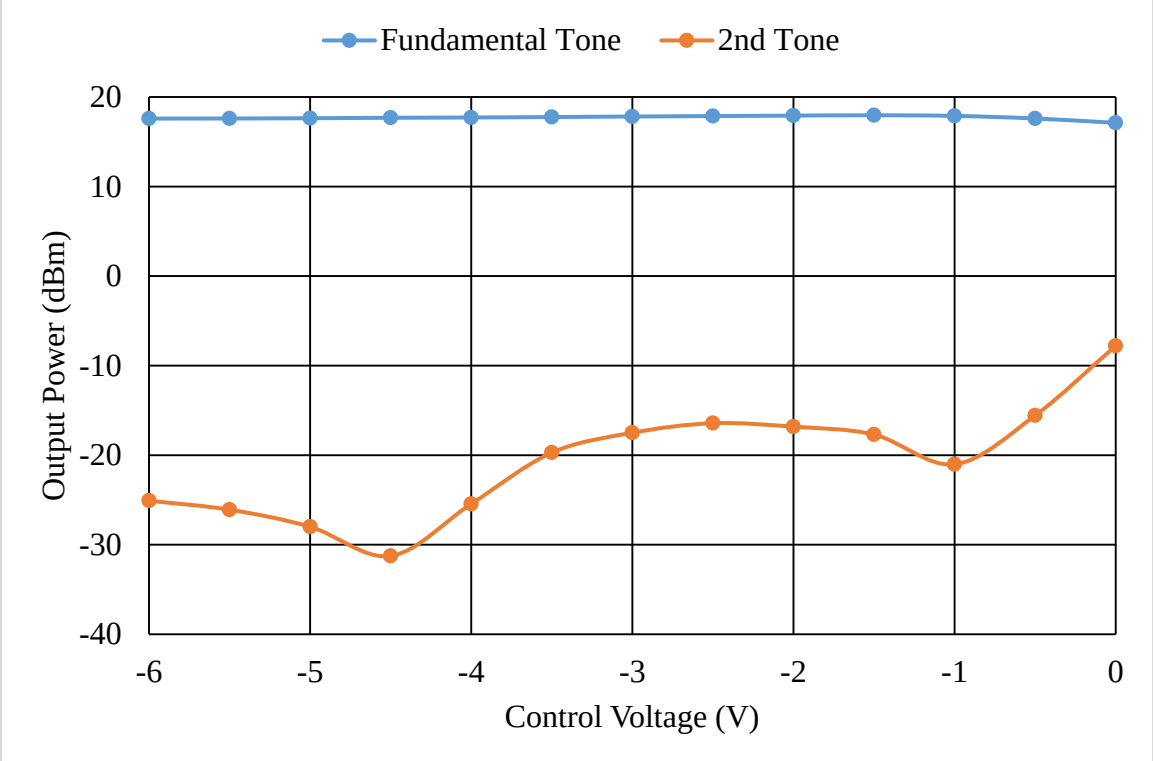

Figure 4.12 Power of fundamental tone and second harmonic at 230 °C

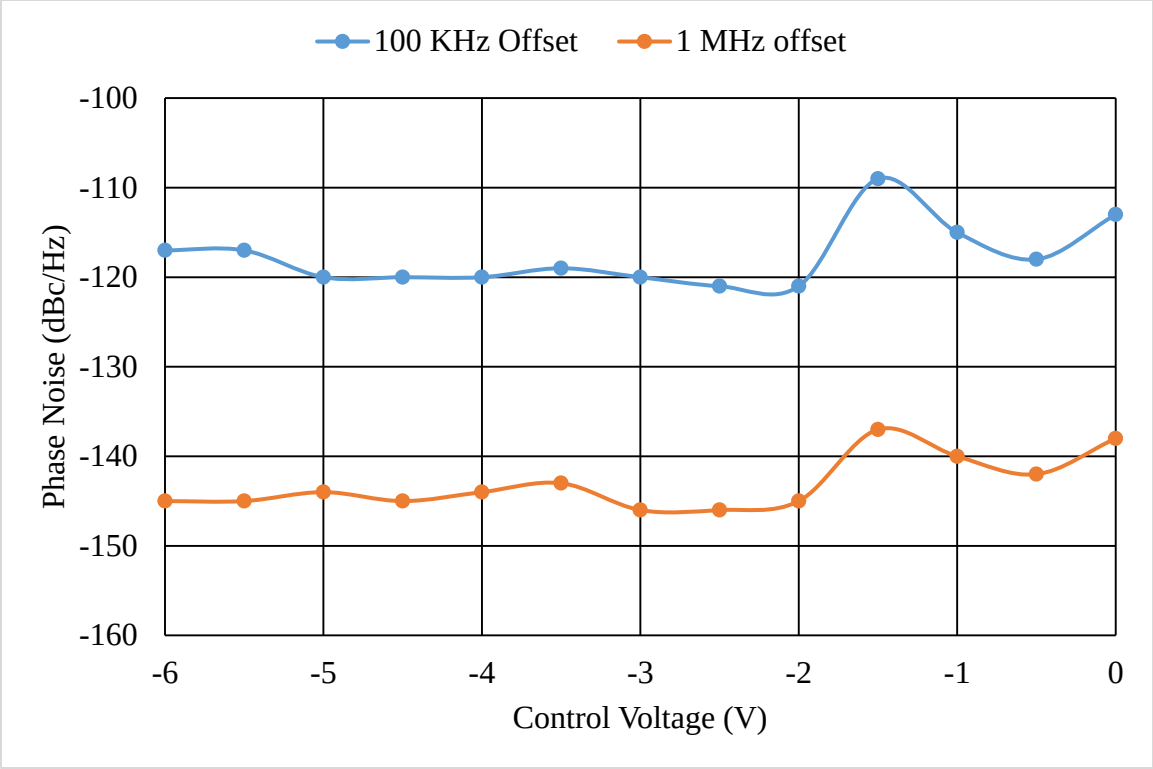

Figure 4.13 Phase noise at 100 KHz and 1 MHz offset

4.2.5 Comparison of VCO Performance at Different Temperature

(a). Operating Frequency

The figure below shows the operating frequency versus control voltage plot at different temperature. At given control voltage, the operating frequency decrease with increasing temperature. The table below lists the lowest and highest operating frequency at different ambient temperature. From 25 °C to 230 °C, the lowest operating frequency decreases by 6.7 MHz and the highest by 7.5 MHz, which indicate a shrink of tuning range of 0.8 MHz.

Table 4-1 Lowest and highest operating frequency at different ambient temperature

Ambient Temperature	Lowest (MHz)	Highest (MHz)	Range(MHz)
25 °C	327.5	367.7	40.2
100 °C	325.2	365.6	40.4
170 °C	322.9	363.0	40.1
230 °C	320.8	360.2	39.4

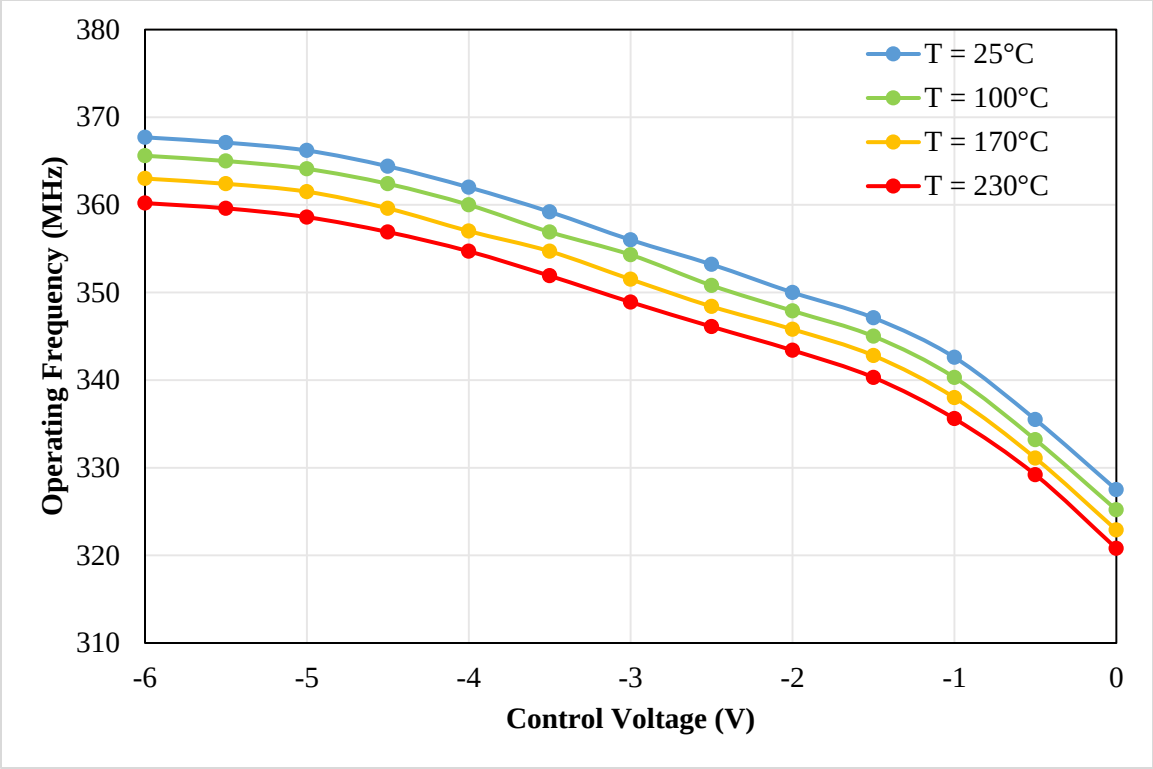

Figure 4.14 Operating frequency range at different temperature

(b). Output Power

The Output Power versus Control Voltage plot is shown in the figure below. The Output Power also decreases with increasing temperature at specific Control Voltage. From 25 °C to 230 °C, the highest output power drops by 1.03 dB and the lowest by 1.05 dB, which results in increasing of variation by 0.02 dB.

Table 4-2 Lowest and highest output power at different temperature

Temperature	Lowest (dBm)	Highest (dBm)	Variation
25 °C	18.16	18.99	0.83
100 °C	17.73	18.40	0.67
170 °C	17.43	18.17	0.74
230 °C	17.11	17.96	0.85

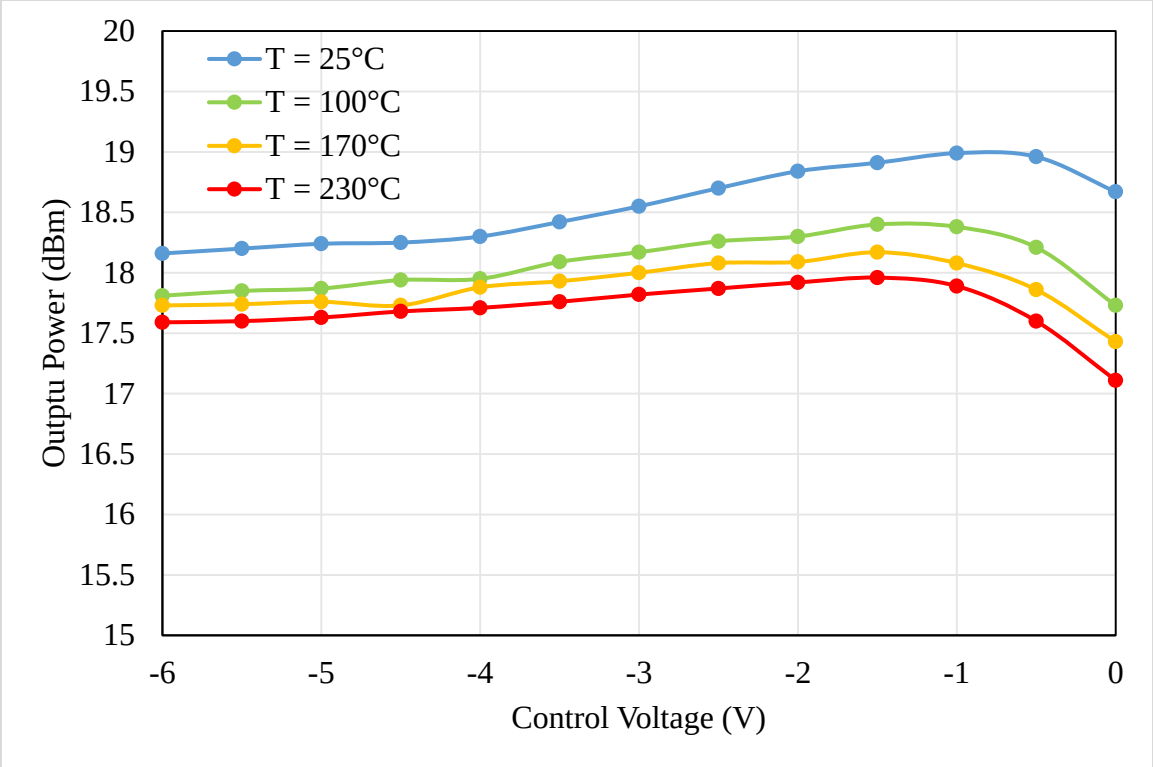

Figure 4.15 Comparison of output power at different temperature

(c). Phase Noise at One Frequency

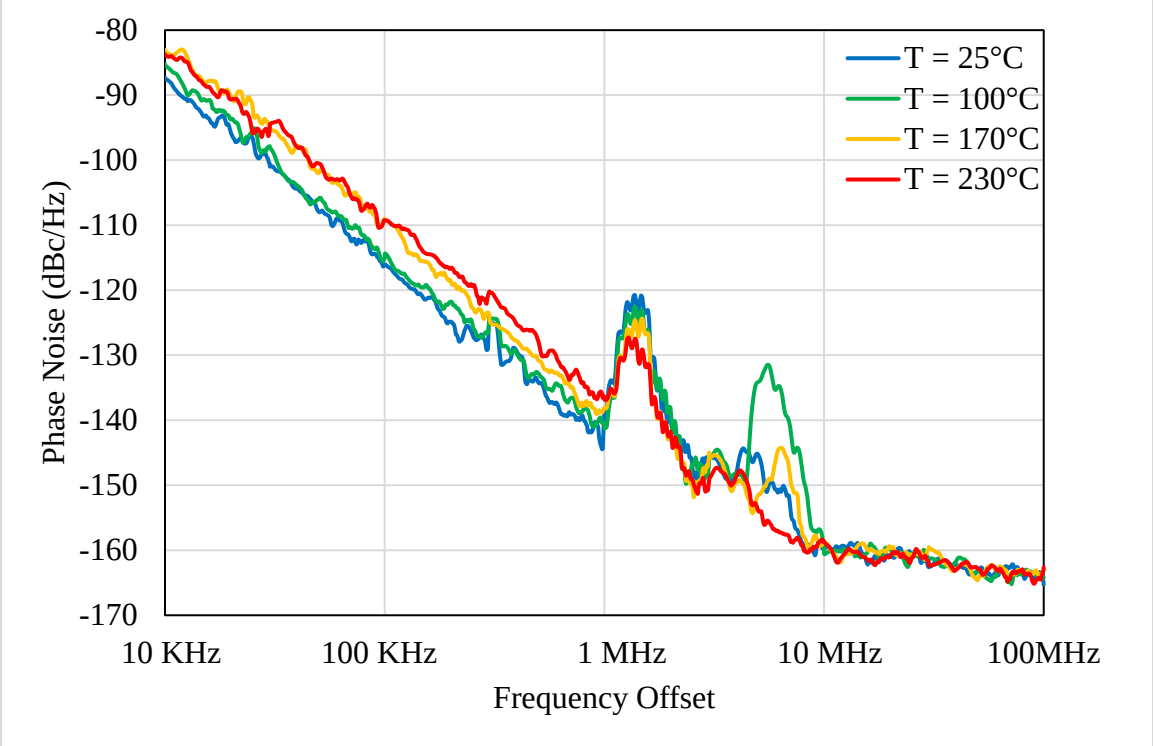

Figure 4.16 Phase noise at center frequency of 340 MHz at different temperature

Chapter 5

5 Conclusion

5.1 Summary

The above work describes the full design process for a 230 °C capable VCO using Colpitts topology. Good performance is exhibited across temperature from 25 °C to 230 °C. The VCO at 230 °C is able to achieve an output power of 17.5 dBm with 0.5 dB variation. The VCO operates at fairly low power for an RF GaN power transistor.

5.2 Conclusions

This work is mainly a proof of concept for high temperature RF circuit using commercial GaN device. It has been in this work that such concept is usable and very good performance is exhibited, which shows potential application environment with high temperature aspect. As oil industry drilling deeper and deeper, growing need for larger communication speed and higher ambient temperature for the device, high temperature RF and microwave circuits will have large room to growth.

5.3 Future work

This work can be improved in several ways. Firstly, the covered frequency range can be increased substantially if better commercial high temperature varactor is available. As in this work, the varactor is made from the transistor, which is expensive and tuning range is small. Secondly, a PLL will be need which incorporated the VCO to achieve better frequency stability and accuracy. Thirdly, this work can be implemented in integrated circuit which will result in smaller size.

References

[1] Schlumberger, Surface systems: Data dilivery, Houston, Texas, Wireless services catalog.

[2] a. H. A. M. J. D. Cressle, Extreme environment electronics, CRC Press, 2012.

[3] A. Dutta-Roy, "An Overview of Cable Modem Technology and Market Perpectives," *IEEE Commun. Mag.*, vol. 39, no. 6, pp. 81-88, 2001.

[4] Z. D. S. a. G. E. Ponchak, "High temperature performance of a SiC MESFET based oscillator," in *IEEE MTT-S Int. Dig.*, Long Beach, CA, 2005.

[5] M. C. S. a. J. L. J. G. E. Ponchak, "30 and 90 MHz oscillators operating through 450 and 470 °C for high temperature wireless sensors," in *Asia-Pacific Microw. Conf. (APMC)*, 2010.

[6] Z. D. S. a. G. E. Ponchak, "1-GHz, 200 °C, SiC MESFET Clapp oscillator," *IEEE Microw. Wireless Compon. Lett.*, vol. 15, pp. 730-732, 2005.

[7] J. M. C. P. Y. a. K. M. L. X. Lu, "A GaN-Based Lamb-Wave Oscillator on Silicon for High-Temperature Integrated Sensors," *IEEE Microw. and Wireless Compon. Lett.*, vol. 23, no. 6, pp. 318-320, 2013.

[8] G. Gonzalez, Foundations of Oscillator Circuit Design, Artech House, Inc, 2007.

[9] A. Grebennikov, RF and Microwave Transistor Oscillator Design, John Wiley & Sons Ltd, 2007.

[10] I. J. Bahl, Fundamentals of RF and Microwave Transistor Amplifiers, John Wiley & Sons, Inc, 2009.

[11] A. Wadsworth, "Fundamentals of Fast Pulsed IV Measurement," Agilent Application Note, 2014.

[12] H. Nagaoka, "The inductance coefficients of solenoids," *Journal of the College of Science,* 1909.

[13] D. W. Knight, "An introduction to the art of Solenoid Inductance Calculation with emphasis on radio-frequency applications," 2016.

[14] G. Johnson, "Tesla Coil Impedance," 2006.